Weak second-order splitting schemes for Lagrangian Monte Carlo particle methods for the composition PDF/FDF transport equations

Haifeng Wang *, Pavel P. Popov, Stephen B. Pope

Sibley School of Mechanical and Aerospace Engineering, Cornell University, Ithaca, NY 14853, USA

A B S T R A C T

We study a class of methods for the numerical solution of the system of stochastic differential equations (SDEs) that arises in the modeling of turbulent combustion, specifically in the Monte Carlo particle method for the solution of the model equations for the composition probability density function (PDF) and the filtered density function (FDF). This system consists of an SDE for particle position and a random differential equation for particle composition. The numerical methods considered advance the solution in time with (weak) second-order accuracy with respect to the time step size. The four primary contributions of the paper are: (i) establishing that the coefficients in the particle equations can be frozen at the mid-time (while preserving second-order accuracy), (ii) examining the performance of three existing schemes for integrating the SDEs, (iii) developing and evaluating different splitting schemes (which treat particle motion, reaction and mixing on different sub-steps), and (iv) developing the method of manufactured solutions (MMS) to assess the convergence of Monte Carlo particle methods. Tests using MMS confirm the second-order accuracy of the schemes. In general, the use of frozen coefficients reduces the numerical errors. Otherwise no significant differences are observed in the performance of the different SDE schemes and splitting schemes.

© 2009 Elsevier Inc. All rights reserved.

1. Introduction

Due to the global concern on energy and environmental issues, developing efficient and accurate numerical combustion tools is highly valuable for increasing our understanding of turbulent reactive systems and hence improving the design of combustion devices with high efficiency and low emissions. During the past several decades, different turbulent combustion models have been devised to represent finite-rate chemistry effects and turbulence-chemistry interactions, e.g., probability density function (PDF) methods [1–3] , flamelet models [4,5], and the conditional moment closure (CMC) [6,7]. PDF methods have proved to be very successful in modeling turbulent combustion (e.g., [8–13]). PDF methods were originally developed in the context of Reynolds Averaged Navier–Stokes Simulations (RANS). Pope [2] introduced the concept of filtered density function (FDF) in the context of large-eddy simulation (LES) [3]. The FDF methods were further developed subsequently by Gao and O'Brien [14], Colucci et al. [15], Jaberi et al. [16] etc. Examples of recent FDF applications can be found in [17–22]. The common practice in FDF methods is to combine the LES solutions for the velocity fields with the composition FDF method. In this work, we only discuss the composition FDF method, while some of the ideas such as designing the second-order splitting schemes are applicable to the joint PDF/FDF of the velocity, composition and additional variables (e.g., the dissipation rate). The FDF in the LES is analogous to the PDF in the RANS. In terms of applications, there is no essential

---

* Corresponding author. Fax: +1 607 255 1222.
  E-mail address: hw98@cornell.edu (H. Wang).

difference between the PDF and the FDF, and almost all the methodologies developed for PDF methods are applicable to FDF methods. Hence, in this discussion, for convenience, we use the PDF to represent both the PDF and the FDF methods when there is no confusion.

Lagrangian Monte Carlo particle methods [1,23] have been widely used to solve the PDF transport equations. In these methods, the continuous PDF is discretized by a finite number of nominal particles, and each particle is governed by a system of stochastic differential equations (SDE) [24] (including an Ito SDE for particle position and a scalar random equation) describing the underlying physical and chemical processes. The numerical solution of SDEs is a much harder problem than that of ordinary differential equations (ODEs). All the well developed high-order ODE schemes degrade to low order of accuracy when applied in Ito SDEs; and, even worse, they can lead to inconsistent schemes because (most) ODE schemes violate the non-anticipatory property of Ito SDEs. Cao and Pope [25] developed a second-order integration scheme for the Ito SDE of particle position arising from the composition PDF transport equations, which considers only position and velocity, not scalars. In this work, we consider the SDE system describing particle transport, molecular mixing and chemical reaction, and develop different weak second-order splitting schemes for the coupled system. To the authors' knowledge, no second-order splitting schemes have previously been developed for the Monte Carlo solution of the coupled SDE system, and have been applied in the RANS/PDF or LES/FDF practice.

Contrary to the supposition of Cao and Pope [25], the weak second-order mid-point Ito SDE scheme turns out to be only first-order accurate when simply coupled with the scalar equations. This is caused by the fact that the predicted mid-point and the final point of the scheme are treated independently and hence the mid-point is not a first-order prediction with the correct conditional probability distribution given the initial and final particle positions. This and other considerations discussed below motivate us to consider other kinds of Ito SDE schemes available in the literature, e.g., predictor–corrector schemes [24,26,27], and Runge–Kutta schemes [24,28–31].

The numerical solution of SDEs is a broad research area. The SDEs can be interpreted in two ways, Ito SDEs and Stratonovich SDEs, and different integration schemes are developed for them, e.g., the Ito SDE schemes [24,26,28–35] and the Stratonovich SDE schemes [27,35–37]. (The Ito SDEs and the Stratonovich SDEs can be readily transformed to each other, so the schemes developed for one type of SDEs are applicable to the other.) In PDF methods, the SDEs are usually interpreted in the Ito view, and this work follows this convention.

Two different types of solutions to SDEs can be sought, the path-wise approximation (strong sense) and the approximation to the probability distribution (weak sense) [24]. In the application of PDF methods, we are more interested in the statistics of the flow fields, so it makes more sense to consider accurate weak solutions for the Monte Carlo particles. Many schemes are developed for this purpose, e.g. [24,26,28–32,34,35,37]. Explicit SDE schemes are usually used for simplicity and efficiency, while implicit schemes can achieve better stability. In this stage of the PDF methods, we only consider the explicit SDE schemes. Implicit SDE schemes may be worthwhile to consider in the future to take advantage of larger time step size. However, with explicit methods we have not experienced any stability problems given that the time step is determined by other factors, e.g., the CFL condition imposed on the solution of the velocity fields by the finite-volume method. The examples of explicit and implicit SDE schemes can be found in [24]. Second-order accuracy is a good compromise between accuracy and efficiency for PDF methods. First-order accuracy is too crude to eliminate numerical uncertainties arising from the modeling of turbulent combustion. The statistical error of the Monte Carlo method scales as $N^{-1/2}$, where N is the number of particles. Due to the slow convergence of the Monte Carlo particle method, most likely the statistical error dominates other numerical errors including the time-stepping error. (In practice, only a small number of particles per cell – on the order of 100 – are used in a RANS/PDF or LES/FDF calculation to make the computation affordable.) Hence using high-order accurate SDE schemes (third-order or higher) in the PDF methods only increases the complexity of the schemes without helping reduce the overall numerical errors.

Many SDE schemes involve derivatives of the coefficients (e.g. [24,25,32]), which increases the difficulty of using them. This makes the derivative-free SDE schemes more attractive, and in fact many derivative-free SDE schemes have been developed (see [24,26–31,34–37]). In this work, we consider three weak second-order SDE schemes, the mid-point scheme of Cao and Pope [25], the predictor–corrector scheme of Kloeden and Platen (pp. 504–506 of [24], also in [26]), and the Runge–Kutta scheme of Tocino and Vigo-Aguiar [30]. The latter two are derivative free. The derivative here refers to the derivative of the drift term, which already includes the derivative of the diffusivity in this work (see Section 2). Hence the Cao and Pope scheme requires the second-order derivative of the diffusivity, and the Kloeden and Platen scheme and the Tocino and Vigo-Aguiar scheme require the first-order derivative of the diffusivity.

In the RANS/PDF simulations, many problems are statistically stationary, and the corresponding Ito SDEs are autonomous, i.e., the drift and diffusion coefficient of the SDEs do not depend on time. Some SDEs schemes are developed only for autonomous SDEs (e.g. [24,26,28,32,34,36]). The LES/FDF simulations are always non-stationary, so the autonomous SDE schemes are generally not applicable,[1] and the non-autonomous SDE schemes [29–32,35,37] are desired. However, it can be verified that solving the non-autonomous SDE system is equivalent up to second-order to solving the SDE system with all the coefficients evaluated at the mid-point of the time step. That is, as far as the weak second-order SDE schemes are concerned, solving the non-autonomous SDE system is equivalent to solving the SDE system with the coefficients frozen at the mid-point using the

---

[1] Adding time as a new variable can make the autonomous SDE schemes applicable. However, this procedure is not favorable because it leads to more evaluations of coefficients in some SDE schemes and hence increases the computational cost.

weak second-order autonomous SDE schemes. Thus, all the weak second-order Ito SDE schemes, no matter whether developed for the autonomous or for the non-autonomous SDEs, are applicable to all the RANS/PDF and LES/FDF applications. Freezing the coefficients in the SDEs at the mid-point is also a big advantage for the staggered arrangement of different fields in the time advancement of the RANS or LES discretization, e.g., in the LES application [38], the velocity fields are staggered in time with the scalars. If the particles are also staggered with the velocity fields (and the turbulent diffusivity) as sketched in Fig. 1, the above freezing the coefficients facilitates the use of the staggered velocity and diffusivity for particle position advancement without interpolation of these quantities in time. (The non-autonomous SDE schemes usually require the evaluation of the drift and diffusion coefficients at different times other than the mid-time [29–32,35,37].) Hence, the complexity of the interface between the RANS or LES solver and the particle solver can be greatly reduced.

To demonstrate the formal order of accuracy and convergence of different numerical schemes, the exact solution of the studied problem, or an accurate estimate of it, is required to provide reference for evaluating the numerical error. For some rare cases, the exact solution to the problem may be obtained with simplification of the problem. This simplification reduces the complexity of the problem, and hence may not be able to represent realistic problems. Given an arbitrary initial condition and other parameters, an accurate numerical solution to a realistic problem is generally available from numerical methods. This accurate numerical solution can be used for error estimation, and has been used in previous studies (e.g., [25]). The method of manufactured solutions (MMS) [39,40] provides a general method for designing test cases with known exact solutions. The test cases can be designed to have the same level of complexity as the real problem. Meanwhile, for the purpose of verification, the manufactured solution need not be related to a physically realistic problem. The idea of MMS is to specify the mathematical solutions *a priori* so that they satisfy a set of augmented governing equations with extra source terms. The augmented governing equations rather than the original ones are solved numerically, and the numerical error is readily evaluated given the (manufactured) exact solutions. The MMS has been used in the verification of different flow solvers [41–44]. In this work, we develop the method of manufactured solutions for the Monte Carlo particle method. The augmented PDF transport equation and the corresponding SDE system are derived. This method is suitable for the verification of the weak convergence of Monte Carlo particle methods.

The developed MMS makes the verification of the Monte Carlo particle method possible. However in practice, this procedure is computationally demanding. A large number of particles are required in the Monte Carlo simulation to make the statistical error negligible compared to the other numerical errors, e.g., the temporal or spatial discretization error. In order to demonstrate the convergence of the weak second-order SDE schemes with respect to time, the computational cost is found to scale as Δt^{-5} (see Section 4.3), where Δt is the time step size. Halving the time step increases the computational cost up to 2^5 times. In this work, in order to make this verification procedure computationally tractable, we perform the simulations in parallel via MPI. In addition, we have to make some simplifications to the test case, which is one-dimensional, constant density, and single scalar. The representativity of the test case and its extension to the full three-dimensional, variable-density and multi-scalar case are discussed at the end of the paper.

The main contributions of the present work are

  (i) The introduction of an SDE system with frozen coefficients (Section 3.2).
 (ii) The comparison of different Ito SDE schemes (Sections 3.3 and 6).
(iii) The development and assessment of different second-order splitting schemes (Sections 5 and 6).
(iv) The development of MMS for the Monte Carlo particle method (Section 4).

The rest of the paper is organized as follows. In Section 2, the composition PDF method and its Monte Carlo solution method are briefly described. In Section 3, the frozen-coefficient SDE system is presented, and several Ito SDE schemes from the literature are discussed. In Section 4, the MMS for the Monte Carlo particle method is developed, and the numerical error and
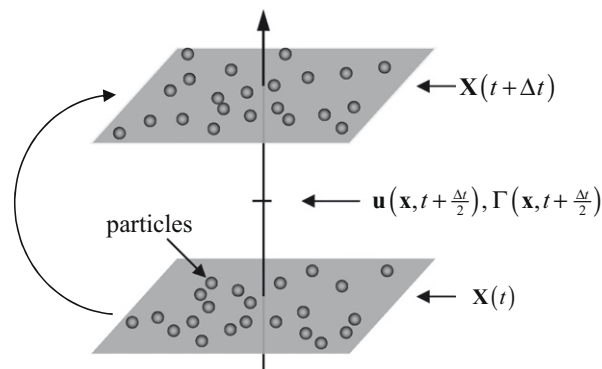
Fig. 1. Sketch of the particle advancement with staggered velocity and diffusivity in time, showing the particle locations **X** at times t and $t + \Delta t$, and the velocity field $\mathbf{u}$ and the turbulent diffusivity field Γ at the half time, $t + \frac{\Delta t}{2}$.

computational cost are briefly discussed. The sub-stepping of the particle scalar equation and the different splitting schemes for the coupled SDE system are discussed in Section 5. The convergence test results of the different splitting schemes and their comparison are shown in Section 6. Further discussion is presented in Section 7, and the conclusions are drawn in Section 8.

2. PDF methods

In this work, only the PDF $f(\psi;\mathbf{x},t)$ of a single scalar $\phi(\mathbf{x},t)$ is considered, where ψ is the sample space variable corresponding to ϕ, and $\mathbf{x}$ and t denote space and time. The modeled transport equation of $f(\psi;\mathbf{x},t)$ takes the following form [1]

$$\frac{\partial f(\psi;\mathbf{x},t)}{\partial t} + \frac{\partial \bar{u}_i(\mathbf{x},t)f(\psi;\mathbf{x},t)}{\partial x_i} = \frac{\partial}{\partial x_i}\left(\Gamma(\mathbf{x},t)\frac{\partial f(\psi;\mathbf{x},t)}{\partial x_i}\right) + \frac{\partial}{\partial \psi}\left(\Omega(\mathbf{x},t)(\psi - \bar{\phi}(\mathbf{x},t))f(\psi;\mathbf{x},t)\right) - \frac{\partial}{\partial \psi}(S(\psi)f(\psi;\mathbf{x},t)), \quad (2.1)$$

where $\mathbf{u} = (u_1, u_2, u_3)$ is the velocity field (satisfying $\nabla \cdot \mathbf{u} = 0$), $\Gamma(\mathbf{x},t)$ is the effective scalar diffusivity (the sum of the molecular diffusivity and the turbulent diffusivity), $\Omega(\mathbf{x},t)$ is the scalar mixing frequency, and $S(\phi)$ is the scalar source term (due to reaction). The overline operation "¯" is the first moment, e.g., $\bar{\phi}$ is the first moment of ϕ. In (2.1), two models are used for the closure, the gradient-diffusion model [3] for the scalar flux (the first term on the right-hand side), and the interaction by exchange with the mean (IEM) mixing model [45] for the conditional dissipation term (the second term on the right-hand side). The IEM model is chosen for simplicity: other mixing models (e.g., modified Curl model [46], EMST model [47]) can be used for the discussion and do not affect the conclusions drawn in this work.

Given $f(\psi;\mathbf{x},t)$, the qth raw moment of the scalar ϕ can be readily obtained as

$$\overline{\phi^q}(\mathbf{x},t) = \int_{-\infty}^{+\infty} \psi^q f(\psi;\mathbf{x},t)\,d\psi. \quad (2.2)$$

From (2.1) and (2.2), we can derive the transport equations for the first moment $\bar{\phi}(\mathbf{x},t)$ and second moment $\overline{\phi^2}(\mathbf{x},t)$

$$\frac{\partial \bar{\phi}(\mathbf{x},t)}{\partial t} + \frac{\partial \bar{u}_i(\mathbf{x},t)\bar{\phi}(\mathbf{x},t)}{\partial x_i} = \frac{\partial}{\partial x_i}\left(\Gamma(\mathbf{x},t)\frac{\partial \bar{\phi}(\mathbf{x},t)}{\partial x_i}\right) + \bar{S}(\mathbf{x},t), \quad (2.3)$$

$$\frac{\partial \overline{\phi^2}(\mathbf{x},t)}{\partial t} + \frac{\partial \bar{u}_i(\mathbf{x},t)\overline{\phi^2}(\mathbf{x},t)}{\partial x_i} = \frac{\partial}{\partial x_i}\left(\Gamma(\mathbf{x},t)\frac{\partial \overline{\phi^2}(\mathbf{x},t)}{\partial x_i}\right) - 2\Omega(\mathbf{x},t)(\overline{\phi^2}(\mathbf{x},t) - \bar{\phi}^2(\mathbf{x},t)) + 2\overline{S\phi}(\mathbf{x},t), \quad (2.4)$$

where $\bar{S}(\mathbf{x},t)$ denotes the mean of $S(\phi(\mathbf{x},t))$. With the definition of $\overline{\phi'^2}(\mathbf{x},t) = \overline{\phi^2}(\mathbf{x},t) - \bar{\phi}^2(\mathbf{x},t)$, the transport equation for $\overline{\phi'^2}(\mathbf{x},t)$ is

$$\frac{\partial \overline{\phi'^2}(\mathbf{x},t)}{\partial t} + \frac{\partial \bar{u}_i(\mathbf{x},t)\overline{\phi'^2}(\mathbf{x},t)}{\partial x_i}$$
$$= \frac{\partial}{\partial x_i}\left(\Gamma(\mathbf{x},t)\frac{\partial \overline{\phi'^2}(\mathbf{x},t)}{\partial x_i}\right) + 2\Gamma(\mathbf{x},t)\frac{\partial \bar{\phi}(\mathbf{x},t)}{\partial x_i}\frac{\partial \bar{\phi}(\mathbf{x},t)}{\partial x_i} - 2\Omega(\mathbf{x},t)\overline{\phi'^2}(\mathbf{x},t) + 2(\overline{S\phi}(\mathbf{x},t) - \bar{S}(\mathbf{x},t)\bar{\phi}(\mathbf{x},t)). \quad (2.5)$$

These moment equations are useful for the verification of weak convergence. For convenience, we refer to $\bar{\phi}(\mathbf{x},t)$ and $\overline{\phi'^2}(\mathbf{x},t)$ as the scalar mean and scalar variance. (In the LES, it is appropriate to call them filtered scalar and sub-filter scalar variance.) Since the first two moments are of most interest in practical applications, we consider only these two moments in the development of MMS for the particle methods in Section 4, and in most discussions of the convergence tests in Section 6. For completeness, for one type of splitting schemes we show the results of weak second-order convergence for the third and fourth moments in Section 6.3.

The PDF Eq. (2.1) can be efficiently solved by the Lagrangian Monte Carlo particle method [1]. A number of nominal particles are introduced to represent the PDF, and each particle carries the properties of the physical position $\mathbf{X}(t)$ and scalar value $\phi(t)$. These properties evolve according to the following set of SDEs [1]

$$d\mathbf{X}(t) = (\bar{\mathbf{u}}(\mathbf{X}(t),t) + \nabla\Gamma(\mathbf{X}(t),t))dt + (2\Gamma(\mathbf{X}(t),t))^{\frac{1}{2}}d\mathbf{W}(t), \quad (2.6)$$

$$\frac{d\phi(t)}{dt} = -\Omega(\mathbf{X}(t),t)(\phi(t) - \bar{\phi}(\mathbf{X}(t),t)) + S(\phi(t)), \quad (2.7)$$

where $\mathbf{W}(t)$ is a standard isotropic Wiener process.

The aim of this work is to design weak second-order numerical schemes for the coupled SDE system (2.6) and (2.7), and to develop the verification procedure to demonstrate the accuracy and convergence of the schemes.

3. Numerical solutions of SDEs

3.1. Ito SDEs and weak convergence

The Ito SDE (2.6) arising from the Monte Carlo particle method has the following general form

$$d\mathbf{X}(t) = \mathbf{D}(\mathbf{X}(t), t)dt + b(\mathbf{X}(t), t)d\mathbf{W}(t), \tag{3.1}$$

for $t \in [0, T]$, where $\mathbf{D}(\mathbf{X}(t), t)$ and $b(\mathbf{X}(t), t)$ are the vector drift and scalar diffusion coefficients, respectively. We assume that the SDE coefficients $\mathbf{D}(\mathbf{X}(t), t)$ and $b(\mathbf{X}(t), t)$ are smooth and measurable functions satisfying a global Lipschitz and a linear growth condition, and all the initial moments of $\mathbf{X}(0)$ exist, so that (3.1) admits the existence and uniqueness of a solution $\mathbf{X}(T)$ (see, e.g., [24]).

Many Ito SDE schemes (e.g. [24,26,28,32,34,36]) have been developed for the autonomous SDEs having the form

$$d\mathbf{X}(t) = \mathbf{D}(\mathbf{X}(t))dt + b(\mathbf{X}(t))d\mathbf{W}(t), \tag{3.2}$$

where the SDE coefficients do not depend directly on time. To take advantage of the autonomous SDE schemes, we will consider an SDE system with frozen coefficients in Section 3.2 which can use the autonomous SDE schemes for our problem (3.1).

We write the particle scalar Eq. (2.7) in the general form

$$\frac{d\phi(t)}{dt} = A(\mathbf{X}(t), \phi(t), t). \tag{3.3}$$

This is a random differential equation due to the randomness of the forcing term $A(\mathbf{X}(t), \phi(t), t)$ (see [24]). Regular ODE schemes can be applied to solve (3.3). Let $\mathbf{Y}(T)$ and $\varphi(T)$ be numerical approximations of the Ito process $\mathbf{X}(T)$ and scalar $\phi(T)$, respectively, where T is the specified stopping time. The weak pth order convergence of the numerical solutions $\mathbf{Y}(T)$ and $\varphi(T)$ to the SDE system (2.6) and (2.7) can be measured by the asymptotic behavior of the numerical error e

$$e = |E(g(\mathbf{Y}(T), \varphi(T), T)) - E(g(\mathbf{X}(T), \phi(T), T))| \leqslant C\Delta t^p, \tag{3.4}$$

where g is a function (chosen to be $\bar{\phi}$ and $\overline{\phi^2}$ in this study), $E(\cdot)$ denotes mathematical expectation, and C is a constant independent of Δt. That is, the largest value of p for which (3.4) holds indicates the order of the scheme.

3.2. SDE system with frozen coefficients

Consider a single step numerical integration $[t_0, t_0 + \Delta t]$ of (3.1) and (3.3), where t_0 is the initial time and Δt is the time step size. It is verified in Appendix A that integrating (3.1) and (3.3) with weak second-order accuracy is equivalent to integrating the following system over the time interval

$$d\mathbf{X}'(t) = \mathbf{D}\left(\mathbf{X}'(t), t_{\frac{1}{2}}\right)dt + b\left(\mathbf{X}'(t), t_{\frac{1}{2}}\right)d\mathbf{W}(t), \tag{3.5}$$

$$\frac{d\phi'(t)}{dt} = A\left(\mathbf{X}'(t), \phi'(t), t_{\frac{1}{2}}\right), \tag{3.6}$$

where $t_\alpha = t_0 + \alpha\Delta t$ $(0 \leqslant \alpha \leqslant 1)$. Over one time step, (3.5) is an autonomous Ito SDE (similar to (3.2)), so any autonomous Ito SDE scheme can be used.

The advantages of this frozen-coefficient SDE system have been discussed in Section 1.

3.3. Weak second-order Ito SDE schemes

In this work, three weak second-order Ito SDE schemes for (3.1) or (3.2) are considered: the mid-point scheme of Cao and Pope [25]; the predictor–corrector scheme of Kloeden and Platen (pp. 504–506 of [24], also in [26]); and, the Runge–Kutta scheme of Tocino and Vigo-Aguiar [30].

In the following discussion, we use $\mathbb{T}$ to denote the transport step (step of the solution to the Ito SDE), and $\mathcal{T}$ to denote the results of the step. We consider the general step from time t_0 to $t_0 + \Delta t$ with initial condition $\mathbf{X}(t_0) = \mathbf{X}_0$.

3.3.1. Scheme of Cao and Pope (CP)

The CP scheme [25] consists of two sub-steps $\mathbb{T}^{cp} = \mathbb{T}_1^{cp}\mathbb{T}_2^{cp}$, where $\mathbb{T}_1^{cp}$ is the prediction of the mid-point and $\mathbb{T}_2^{cp}$ is the final solution.

First CP sub-step $\mathbb{T}_1^{cp}$:

$$\mathbf{Y}\left(t_{\frac{1}{2}}\right) = \mathbf{X}_0 + \mathcal{T}_1^{cp}(\mathbf{X}_0, t_0, \Delta t, \zeta) \tag{3.7}$$

with $\mathcal{T}_1^{cp}(\mathbf{X}, s, \Delta t, \zeta) = \frac{\Delta t}{2} \cdot \mathbf{D}(\mathbf{X}, s) + \left(\frac{1}{2}\Delta t\right)^{\frac{1}{2}}b(\mathbf{X}, s)\zeta$, where ζ is a standardized Gaussian random vector (each component of ζ is an independent Gaussian random number with zero mean and unit variance).

Second CP sub-step $\mathbb{T}_2^{cp}$:

$$\mathbf{Y}(t_1) = \mathbf{Y}\left(t_{\frac{1}{2}}\right) + \mathcal{T}_2^{cp}\left(\mathbf{X}_0, \mathbf{Y}\left(t_{\frac{1}{2}}\right), t_{\frac{1}{2}}, \Delta t, \xi, \eta\right) \tag{3.8}$$

with $\mathcal{T}_2^{cp}(\mathbf{X}, \mathbf{Y}, s, \Delta t, \xi, \eta) = \left(\mathcal{T}_{2,1}^{cp}, \mathcal{T}_{2,2}^{cp}, \mathcal{T}_{2,3}^{cp}\right)$, and

$$\mathcal{T}_{2,i}^{\mathrm{cp}}(\mathbf{X},\mathbf{Y},s,\Delta t,\xi,\boldsymbol{\eta}) = \Delta t D_i(\mathbf{Y},s) + \left(\frac{1}{2}\Delta t\right)^{\frac{1}{2}} b(\mathbf{Y},s)(\xi_i + \eta_i) + \Delta t b(\mathbf{Y},s)\frac{\partial b(\mathbf{Y},s)}{\partial X_j}(\eta_i\eta_j - \delta_{ij})$$

$$- \left(\frac{1}{2}\Delta t\right)^{\frac{3}{2}}\left[b(\mathbf{Y},s)\left(\frac{\partial b(\mathbf{Y},s)}{\partial X_i}\frac{\partial b(\mathbf{Y},s)}{\partial X_j} + \frac{\partial b(\mathbf{Y},s)}{\partial X_k}\frac{\partial b(\mathbf{Y},s)}{\partial X_k}\delta_{ij}\right)\right.$$

$$\left. -b(\mathbf{Y},s)\left(\frac{\partial D_i(\mathbf{Y},s)}{\partial X_j} + \frac{\partial D_j(\mathbf{Y},s)}{\partial X_i}\right)\right](\xi_j + \eta_j) + X_i - Y_i, \tag{3.9}$$

where ξ and $\boldsymbol{\eta}$ are two independent standardized Gaussian random vectors, and δ_{ij} is the Kronecker delta.

The overall CP step can be re-expressed as

$$\mathbf{Y}(t_1) = \mathbf{X}_0 + \mathcal{T}^{\mathrm{cp}}\left(\mathbf{X}_0, t_0, t_{\frac{1}{2}}, \Delta t, \zeta, \xi, \boldsymbol{\eta}\right), \tag{3.10}$$

where

$$\mathcal{T}^{\mathrm{cp}}(\mathbf{X}, s_1, s_2, \Delta t, \zeta, \xi, \boldsymbol{\eta}) = \mathcal{T}_2^{\mathrm{cp}}\left(\mathbf{X}, \mathbf{Y}_{\frac{1}{2}}, s_2, \Delta t, \xi, \boldsymbol{\eta}\right) - \mathbf{X} + \mathbf{Y}_{\frac{1}{2}} \tag{3.11}$$

with $\mathbf{Y}_{\frac{1}{2}} = \mathbf{X} + \mathcal{T}_1^{\mathrm{cp}}(\mathbf{X}, s_1, \Delta t, \zeta)$.

The application of CP to the frozen-coefficient system is given by (3.10) and (3.11), but with s_1 and s_2 set to $t_{\frac{1}{2}}$ in (3.11).

3.3.2. Scheme of Kloeden and Platen (KP)

The KP scheme $\mathbb{T}^{\mathrm{kp}}$ [24,26] is a scheme of predictor–corrector type for autonomous Ito SDEs. The one-dimensional KP scheme is the following (the multi-dimensional KP scheme can be found in the same reference)

$$Y(t_1) = X_0 + \mathcal{T}^{\mathrm{kp}}(X_0, \Delta t, \xi) \tag{3.12}$$

with $\mathcal{T}^{\mathrm{kp}}(X, \Delta t, \xi) = \frac{1}{2}(D(Y_a) + D(X))\Delta t + Y_b$, and

$$Y^{\pm} = X_0 + D(X_0)\Delta t \pm b(X_0)\Delta t^{\frac{1}{2}},$$

$$Y_c = X_0 + D(X_0)\Delta t + b(X_0)\Delta t^{\frac{1}{2}}\xi,$$

$$Y_b = \frac{1}{4}[b(Y^+) + b(Y^-) + 2b(X_0)]\Delta t^{\frac{1}{2}}\xi + \frac{1}{4}[b(Y^+) - b(Y^-)]\Delta t^{\frac{1}{2}}(\xi^2 - 1),$$

$$Y_a = X_0 + \frac{1}{2}(D(Y_c) + D(X_0))\Delta t + Y_b,$$

and ξ is either a standardized Gaussian random number or a three-point distributed random number with probability

$$\mathrm{Prob}\left(\xi = \pm\sqrt{3}\right) = \frac{1}{6}, \quad \mathrm{Prob}(\xi = 0) = \frac{2}{3}. \tag{3.13}$$

This autonomous Ito SDE scheme is applicable only to the frozen-coefficient SDE (3.5).

3.3.3. Scheme of Tocino and Vigo-Aguiar (TV)

Tocino and Vigo-Aguiar [30] proposed a family of weak second-order Runge–Kutta Ito SDE schemes. The one-dimensional version of TV scheme $\mathbb{T}^{\mathrm{tv}}$ for non-autonomous SDEs is shown in the following (the multi-dimensional version can be found in the same reference)

$$Y(t_1) = X_0 + \mathcal{T}^{\mathrm{tv}}(X_0, \Delta t, t_0, \mu_0, \bar{\mu}_0, \xi), \tag{3.14}$$

where ξ is a standardized Gaussian random number and

$$\mathcal{T}^{\mathrm{tv}}(X, \Delta t, s, \mu_0, \bar{\mu}_0, \xi) = (\alpha_1 k_0 + \alpha_2 k_1)\Delta t + (\gamma_1\xi + \gamma_2 + \gamma_3\xi^2)\Delta t^{1/2}s_0 + (\lambda_1\xi + \lambda_2 + \lambda_3\xi^2)\Delta t^{1/2}s_1 + (\mu_1\xi + \mu_2 + \mu_3\xi^2)\Delta t^{1/2}s_2, \tag{3.15}$$

where

$$k_0 = D(X, s),$$

$$s_0 = b(X, s),$$

$$k_1 = D(X + \lambda_0 k_0\Delta t + (\nu_1\xi + \nu_2\xi^3)\Delta t^{1/2}s_0, s + \mu_0\Delta t),$$

$$s_1 = b(X + \bar{\lambda}_0 k_0\Delta t + (\beta_1\xi + \beta_2 + \beta_3\xi^2)\Delta t^{1/2}s_0, s + \bar{\mu}_0\Delta t),$$

$$s_2 = b(X + \bar{\lambda}_0 k_0\Delta t + (\delta_1\xi + \delta_2 + \delta_3\xi^2)\Delta t^{1/2}s_0, s + \bar{\mu}_0\Delta t).$$

The example of the two-parameter (α_2 and μ_3) families of the TV scheme are

$$\alpha_1 = 1 - \alpha_2, \quad \mu_0 = \lambda_0 = \frac{1}{2\alpha_2}, \quad \nu_2 = \pm \frac{\sqrt{2\alpha_2 - 1}}{2\sqrt{6}\alpha_2}, \quad \nu_1 = \frac{1}{2\alpha_2} - 3\nu_2$$

with $\alpha_2 \geqslant 1/2$, and either

$$\beta_3 = \delta_3 = 0, \quad \bar{\mu}_0 = \bar{\lambda}_0 = 1, \quad \gamma_1 = \frac{1}{2}, \quad \gamma_2 = \gamma_3 = 0, \quad \mu_1 = \lambda_1 = \frac{1}{4},$$

$$\mu_2 = -\lambda_2 = \frac{1 - 48\mu_3^2}{32\mu_3}, \quad \lambda_3 = -\mu_3, \quad \beta_2 = -\delta_2 = \frac{8\mu_3}{1 - 48\mu_3^2}, \quad \beta_1 = \delta_1 = 1 + \frac{32\mu_3^2}{1 - 48\mu_3^2},$$

(3.16)

with $\mu_3 \neq 0$ and $\mu_3 \neq \frac{1}{4\sqrt{3}}$, or

$$\beta_1 = \beta_2 = \delta_1 = \delta_2 = 0, \quad \gamma_2 = \gamma_3 = 0, \quad \gamma_1 = 1 - \frac{24\mu_3^2}{5}, \quad \mu_1 = \lambda_1 = \frac{12\mu_3^2}{5},$$

$$\bar{\mu}_0 = \bar{\lambda}_0 = \frac{5}{48\mu_3^2}, \quad \delta_3 = -\beta_3 = \frac{1}{12\mu_3}, \quad \lambda_2 = -\mu_2 = 3\mu_3, \quad \lambda_3 = -\mu_3,$$

(3.17)

with $\mu_3 \neq 0$. In the results presented in Section 6, the values of $\alpha_2 = 1.0$ and $\mu_3 = 0.5$ and (3.17) are used. The effect of choosing the different constants and different families of the parameters is discussed in Section 7.

When $s = t_{\frac{1}{2}}$ and $\mu_0 = \bar{\mu}_0 = 0$ in (3.15), this scheme is applicable to the frozen-coefficient Ito SDE (3.5).

The CP scheme (3.10) involves the spatial derivatives of coefficients, while KP scheme (3.12) and TV scheme (3.14) are derivative-free.

In this section, the numerical solution to the Ito SDEs (3.1) and (3.5) is discussed. Below (in Section 5), we discuss the numerical solution to the scalar Eq. (2.7) and the splitting schemes of the coupled system (2.6) and (2.7). Before discussing the solution of the scalar equation, in the next section we first develop the method of manufactured solutions (MMS) for the particle method, and derive the augmented particle scalar equation for the purpose of verification.

4. Method of manufactured solutions (MMS) for Monte Carlo particle methods

A numerical test case with known exact solutions (or with highly accurate numerical solutions via other methods) is often required for validating models and algorithms and for verifying the computer programming. MMS [39,40] provides a general procedure for generating an analytical solution for this purpose. MMS was primarily used in the verification of the numerical solution of partial differential equations (PDEs) with finite-difference, finite-volume, and finite-element based numerical methods in the past [41–44]. In that practice, the analytical solutions to the equations to be solved were manufactured. In the current Monte Carlo particle method, however, we need the analytical solutions to the quantities which are not directly solved, i.e., the SDE system (2.6) and (2.7) is solved numerically, while the moments of the scalar $\overline{\phi^q}$ are used for examining the weak convergence. In the following, we first obtain the augmented PDEs admitting the manufactured solutions of scalar moments, then derive the augmented SDE system consistent with the augmented PDEs. In principle, any order of scalar moment should be tested for convergence. However, this is technically impractical. In this work, we consider mostly the first and second moments of the scalar, which are the primary interest of PDF applications. For one case, we present the convergence results for the third and fourth moments (Section 6.3). The analysis of the schemes discussed in this paper indicates that they are all convergent (with first or second-order accuracy) for the PDF and hence for all moments. This convergence has been verified for the first four moments, and there is no reason to doubt that higher moments converge similarly.

4.1. Augmented SDE system for MMS

In this work, we consider the manufactured solutions only for the scalar mean and variance. In the transport equations for the scalar mean $\bar{\phi}$ (2.3) and variance $\overline{\phi'^2}$ (2.5), the terms containing the reaction source term $S(\phi)$ are generally unclosed because of the non-linearity of the reaction term. Closing these equations requires that $\overline{S\phi}(\mathbf{x}, t)$ and $\overline{S}(\mathbf{x}, t)$ be known in terms of $\bar{\phi}$ and $\overline{\phi'^2}$, which in turn requires $S(\phi)$ to be linear in ϕ. Hence, for verification purposes, we specify the following linear relation

$$S(\phi) = R_a(\phi(\mathbf{x}, t) - R_b),$$

(4.1)

in which R_a and R_b are specified constants. Substituting the above equation into (2.3) and (2.5), we see that those equations become closed.

We need analytical solutions for $\bar{\phi}$ and $\overline{\phi'^2}$ to (2.3) and (2.5) for the error estimate in the convergence study. In general, these analytical solutions cannot be obtained. The idea of the MMS is to specify analytical functions of $\bar{\phi}_m$ and $\overline{\phi'^2}_m$ in advance, where the subscript "m" denotes manufactured solution. These functions certainly do not satisfy (2.3) and (2.5) in general. They satisfy the following augmented equations with extra source terms (S_m and S_v) compared to the original ones

$$\frac{\partial \bar{\phi}_m(\mathbf{x},t)}{\partial t} + \frac{\partial \bar{u}_i(\mathbf{x},t)\bar{\phi}_m(\mathbf{x},t)}{\partial x_i} = \frac{\partial}{\partial x_i}\left(\Gamma(\mathbf{x},t)\frac{\partial \bar{\phi}_m(\mathbf{x},t)}{\partial x_i}\right) + R_a(\bar{\phi}_m(\mathbf{x},t) - R_b) + S_m(\mathbf{x},t),\tag{4.2}$$

$$\frac{\partial \overline{\phi'^2}_m(\mathbf{x},t)}{\partial t} + \frac{\partial \bar{u}_i(\mathbf{x},t)\overline{\phi'^2}_m(\mathbf{x},t)}{\partial x_i}$$

$$= \frac{\partial}{\partial x_i}\left(\Gamma(\mathbf{x},t)\frac{\partial \overline{\phi'^2}_m(\mathbf{x},t)}{\partial x_i}\right) + 2\Gamma(\mathbf{x},t)\frac{\partial \bar{\phi}_m(\mathbf{x},t)}{\partial x_i}\frac{\partial \bar{\phi}_m(\mathbf{x},t)}{\partial x_i} - 2\Omega(\mathbf{x},t)\overline{\phi'^2}_m(\mathbf{x},t) + 2R_a\overline{\phi'^2}_m(\mathbf{x},t) + S_v(\mathbf{x},t).\tag{4.3}$$

The forcing terms S_m and S_v are determined from the above equations, given the specifications for all the other functions in the equations. We now turn our attention to a problem satisfying the above Eqs. (4.2) and (4.3).

Due to the extra source terms, the above Eqs. (4.2) and (4.3) are no longer consistent with the PDF Eq. (2.1) and the particle Eqs. (2.6) and (2.7). A consistent PDF equation can be obtained in the following

$$\frac{\partial f(\psi;\mathbf{x},t)}{\partial t} + \frac{\partial \bar{u}_i(\mathbf{x},t)f(\psi;\mathbf{x},t)}{\partial x_i}$$

$$= \frac{\partial}{\partial x_i}\left(\Gamma(\mathbf{x},t)\frac{\partial f(\psi;\mathbf{x},t)}{\partial x_i}\right) + \frac{\partial}{\partial \psi}(\Omega(\mathbf{x},t)(\psi - \bar{\phi}_m(\mathbf{x},t))f(\psi;\mathbf{x},t)) - \frac{\partial}{\partial \psi}(R_a(\psi - R_b)f(\psi;\mathbf{x},t))$$

$$- S_m(\mathbf{x},t)\frac{\partial f(\psi;\mathbf{x},t)}{\partial \psi} + \frac{\partial}{\partial \psi}(\Omega_v(\mathbf{x},t)(\psi - \bar{\phi}_m(\mathbf{x},t))f(\psi;\mathbf{x},t))\tag{4.4}$$

where $\Omega_v(\mathbf{x},t) = -S_v(\mathbf{x},t)/(2\overline{\phi'^2}_m(\mathbf{x},t))$ is a scalar-frequency-like quantity due to the source term S_v. (Notice that $\Omega_v(\mathbf{x},t)$ can be negative.) The implementation of the IEM model is adapted to account for the effect of Ω_v to obtain the correct variation rate of scalar variance. Other mixing models (e.g. modified Curl or EMST) are not appropriate for this term when $\Omega_v(\mathbf{x},t)$ becomes negative. The corresponding (augmented) particle scalar equation is then

$$\frac{d\phi(t)}{dt} = -\Omega(\mathbf{X}(t),t)(\phi(t) - \bar{\phi}_m(\mathbf{X}(t),t)) + R_a(\phi(t) - R_b) + S_m(\mathbf{X}(t),t) - \Omega_v(\mathbf{X}(t),t)(\phi(t) - \bar{\phi}_m(\mathbf{X}(t),t)).\tag{4.5}$$

The four terms on the right-hand side represent the molecular mixing process $\mathbb{M}$, reaction process $\mathbb{R}$, scalar mean forcing process $\mathbb{S}$, and scalar variance forcing process $\mathbb{V}$, respectively. This equation can be simplified, e.g., by combining $\mathbb{M}$ and $\mathbb{V}$, but we generally do not combine them due to the physical difference of each process and due to the flexibility of implementing different sub-models for each process (e.g., using other mixing models for $\mathbb{M}$).

The particle position Eq. (2.6) deals with the convection and diffusion of the PDF which are not changed in (4.4), so (2.6) remains the same after using the MMS. The particle equations to be considered now become (2.6) and (4.5).

A particular MMS test case requires the specification of $\bar{\phi}_m(\mathbf{x},t), \overline{\phi^2}_m(\mathbf{x},t), \bar{u}(\mathbf{x},t), \Gamma(\mathbf{x},t), S_m(\mathbf{x},t), S_v(\mathbf{x},t)$, and $\Omega(\mathbf{x},t)$. In Appendix C, these specifications are given for the tests used in this study.

4.2. Error analysis for weak convergence

The manufactured solutions to the first two moments of the scalar are discussed in the previous sub-section. Here, we discuss how to use these solutions to measure the numerical error.

We consider a one-dimensional problem, and the computational domain $[0, L_0]$ is partitioned into I cells $\left[x_i - \frac{\Delta x_i}{2}, x_i + \frac{\Delta x_i}{2}\right]$, $i = 1, \ldots, I$, where x_i is the center of the ith grid cell and Δx_i is the cell size. The grid used for the error analysis is often the same as the grid used in the finite-volume method of the flow fields which is generally non-uniform. The volume average $\langle \overline{\phi^q} \rangle_i$ of the qth scalar moment in the ith cell is

$$\langle \overline{\phi^q} \rangle_i = \frac{1}{\Delta x_i} \int_{x_i - \frac{\Delta x_i}{2}}^{x_i + \frac{\Delta x_i}{2}} \overline{\phi^q}_m(x,T)dx,\tag{4.6}$$

where $\langle \cdot \rangle$ denotes volume average and $\overline{\phi^q}_m(x,t)$ is the manufactured solution. The volume average $\langle \overline{\phi^q} \rangle$ is used as the exact solution in (3.4) to evaluate the numerical error of the particle method.

The Monte Carlo particle method involves the tracking of many particles governed by (2.6) and (4.5). To obtain accurate estimates of scalar moments, a very large number of particles is required (e.g., up to the order of 10^{10}) for the currently considered test case (with a small time step). The exact required number of particles is not known in advance. We perform the convergence tests with an adaptive number of particles, i.e., we perform the simulation with a fixed number of particles (e.g., 10^4) and repeat the trials independently many times as needed (e.g., repeat 10^6 times to achieve 10^{10} particles for the above case).

The numerical approximation to $\langle \overline{\phi^q} \rangle_i$ can be estimated from the ensemble average of the particles in the cell

$$\langle \overline{\phi^q} \rangle_{i,k}^* = \frac{1}{N_{i,k}} \sum_{n=1}^{N_{i,k}} \phi_{n,i,k}^q(T),\tag{4.7}$$

where $\phi_{n,i,k}$ is the scalar value of the nth particle in the ith cell for the kth trial, $N_{i,k}$ is the number of particles in the cell for the kth trial, and $\langle \cdot \rangle^*$ denotes an ensemble average.

The numerical error in predicting the qth scalar moment for the ith cell on the kth trial is then measured as

$$e_{q,i,k} = \langle \overline{\phi^q} \rangle^*_{i,k} - \langle \overline{\phi^q} \rangle_i. \tag{4.8}$$

For the finite number of particles in the simulation, the numerical error $e_{q,i,k}$ is a random variable with an approximately Gaussian distribution, and can be decomposed as

$$e_{q,i,k} = \mu_{q,i} + \sigma_{q,i} \xi_{q,i,k}, \tag{4.9}$$

(with no implied summation), where $\mu_{q,i} \equiv E(e_{q,i,k})$, $\sigma^2_{q,i} \equiv \text{var}(e_{q,i,k})$, and $\xi_{q,i,k}$ is a standardized Gaussian random variable ($\langle \xi_{q,i,k} \rangle = 0, \text{var}(\xi_{q,i,k}) = 1$), which is independent on each trial ($\langle \xi_{q,i,k} \xi_{q,i,l} \rangle = 0, k \neq l$), but not necessarily from cell to cell ($\langle \xi_{q,i,k} \xi_{q,l,k} \rangle \neq 0$). The deterministic error $\mu_{q,i}$ consists of two possible sources: the time-stepping error (which scales as Δt^2 for second-order schemes), and the bias error (which scales as N^{-1}_{trial} [23], N_{trial} being the number of particles per trial). In this study, the number of particles is on the order of 10^4, and the results reported in Section 6 support the supposition that the bias error is small compared to the time-stepping error (for the smallest time step $\Delta t/T = \frac{1}{40}$). The statistical error $\sigma_{q,i}$ scales as $N^{-1/2}$ in which N is the total number of particles used in a convergence test.

We define a global error $\mathcal{E}_{\overline{\phi^q}}$,

$$E(\mathcal{E}_{\overline{\phi^q}}) \equiv \left[\frac{1}{I} \sum_{i=1}^{I} \mu^2_{q,i} \right]^{1/2}, \tag{4.10}$$

which, in the case of an infinite number of trials, is the two-norm (over the cells) of the expectation of $e_{q,i,k}$. In Appendix B we describe the construction of an un-biased estimate of $\mathcal{E}_{\overline{\phi^q}}$ based on a finite number of trials.

We use the global measure of error $\mathcal{E}_{\overline{\phi^q}}$ to investigate the numerical accuracy and convergence. The global error uses all the particles from the simulation, so it presumably involves less statistical error than the local error which uses a small portion of particles from the simulations, although the cell-to-cell estimates of the local error are not independent. Due to the random nature of the global error, multiple sets of trials are performed to estimate the mean and variance of $\mathcal{E}_{\overline{\phi^q}}$, and hence to estimate the confidence interval of the error.

4.3. Computational cost of a Monte Carlo convergence study

In this sub-section, we give an estimate of the computational requirement for verifying the convergence of the Monte Carlo method. In this work, we are primarily interested in the time-stepping error. The computational cost of the Monte Carlo simulation is proportional to the number of particles multiplied by the time steps taken. From the previous discussion, we know that the mean and standard deviation of the error scale as $\mu_{q,i} \approx C_\mu \Delta t^p$ and $\sigma_{q,i} \approx C_\sigma N^{-1/2}$, so (4.9) becomes

$$e_{q,i,k}(\overline{\phi^q}) \approx C_\mu \Delta t^p + C_\sigma \frac{1}{N^{1/2}} \xi_{i,k}, \tag{4.11}$$

where C_μ and C_σ are constants.

To show the numerical convergence of $e_{q,i,k}$ with respect to the time step Δt, we require that the time-stepping error dominates the statistical error in (4.11), i.e., $C_\mu \Delta t^p \gg C_\sigma N^{-1/2}$. The ratio between the statistical error and the time-stepping error is

$$C_r = C_\sigma N^{-1/2} / C_\mu \Delta t^p \ll 1, \tag{4.12}$$

where C_r is a constant, then

$$N = C^2_\sigma C^{-2}_\mu C^{-2}_r \Delta t^{-2p}. \tag{4.13}$$

The total number of time steps taken is $N_t = T/\Delta t$, so then the computational cost F for verifying Monte Carlo convergence scales as

$$F = N \cdot N_t = C^2_\sigma T C^{-2}_\mu C^{-2}_r \Delta t^{-2p-1} \propto \Delta t^{-2p-1}. \tag{4.14}$$

For weak second-order numerical schemes ($p = 2$), the computational cost F scales as Δt^{-5}. Hence to make the computation affordable, simplification is made on the test case as discussed in Section 1, i.e., one-dimensional, constant density, and single scalar.

In this section, the MMS for the Monte Carlo particle method is developed. The error analysis and the computational cost are discussed. The manufactured analytical solutions to the one-dimensional problem for convergence test is designed and shown in Appendix C.

5. Weak second-order splitting schemes

In this section, we develop the weak second-order splitting schemes for the coupled SDE system (3.1) and (3.3) (and the frozen-coefficient system (3.5) and (3.6)). To construct second-order splitting schemes for the coupled system, a necessary condition is to have the SDE and the scalar equation each integrated with at least second-order accuracy. The (weak) second-

order schemes to the SDE have been discussed in Section 3.3. In the following, different second-order splitting schemes for the scalar equation are first discussed, and then the splitting schemes for the coupled SDE system.

5.1. Sub-stepping of scalar evolution

The augmented particle scalar Eq. (4.5) can be solved by ODE schemes. As discussed in Section 4.1, this equation describes four processes (mixing $\mathbb{M}$, reaction $\mathbb{R}$, scalar mean forcing $\mathbb{S}$, and scalar variance forcing $\mathbb{V}$), and sub-stepping is often used to solve this kind of equation, i.e., splitting (4.5) into the following four equations to solve separately with each describing one process,

$$\mathbb{M} : \frac{d\phi(t)}{dt} = -\Omega(\mathbf{X}(t),t)(\phi(t) - \bar{\phi}(\mathbf{X}(t),t)), \tag{5.1}$$

$$\mathbb{R} : \frac{d\phi(t)}{dt} = +R_a(\phi(t) - R_b), \tag{5.2}$$

$$\mathbb{S} : \frac{d\phi(t)}{dt} = +S_m(\mathbf{X}(t),t), \tag{5.3}$$

$$\mathbb{V} : \frac{d\phi(t)}{dt} = -\Omega_\nu(\mathbf{X}(t),t)(\phi(t) - \bar{\phi}(\mathbf{X}(t),t)). \tag{5.4}$$

Consider one step of integration over the time interval $[t_0, t_0 + \Delta t]$ from the initial condition $\phi_0 = \phi(t_0)$. The numerical solution $\varphi(t)$ to the above four equations can be obtained as following.

Mixing sub-step $\mathbb{M}$**:** In (5.1), if Ω and $\bar{\phi}$ are frozen at some particle position $\mathbf{X}(r)$ and time s ($r, s \in [t_0, t_0 + \Delta t]$), then the analytical solution to the mixing sub-step is

$$\varphi(t_1) = \mathcal{M}(\phi_0, \mathbf{X}(r), s, \Delta t) = \bar{\phi}(\mathbf{X}(r), s) + (\phi_0 - \bar{\phi}(\mathbf{X}(r), s)) \exp(-\Omega(\mathbf{X}(r), s)\Delta t). \tag{5.5}$$

For the splitting schemes of the SDE system (3.1) and (3.3), we require the time r to be equal to s to evaluate the coefficients Ω and $\bar{\phi}$, and the time (r and s) can be specified for different schemes, e.g., $r = s = t_0$ for explicit schemes, $t_0 < r = s \leqslant t_1$ for implicit schemes, where $t_\alpha = t_0 + \alpha\Delta t$ ($0 \leqslant \alpha \leqslant 1$). Second-order accuracy can be achieved by choosing $r = s = t_{\frac{1}{2}}$. When used in solving the frozen-coefficient scalar Eq. (3.6), the time in (5.5) is $s = t_{\frac{1}{2}}$, while the time r can be different from s. The particle position $\mathbf{X}(r)$ at time r for the evaluation of the scalar coefficients is the result of the previous transport sub-step, and is available only at three times $r = t_0, t_{\frac{1}{2}}$ and t_1 in a second-order splitting scheme (with the exceptions of $\mathbb{T}^{\text{cp}}\mathbb{C}\mathbb{R}\mathbb{C}'\mathbb{T}^{\text{cp}}$ and $\mathbb{T}^{\text{cp}}\mathbb{C}\mathbb{R}\mathbb{C}'\mathbb{T}^{\text{cp}}$-F in Section 5.2 in which $\mathbf{X}$ is available also at $r = t_{\frac{1}{4}}$ and $t_{\frac{3}{4}}$). The meaning of r and s is the same for the other sub-steps.

The scalar mean $\bar{\phi}(\mathbf{X}, s)$ can be approximated by the cell mean of particles at time s. During the mixing sub-step (and the scalar variance forcing sub-step), the scalar mean is preserved, and so the scalar mean is the same at different times within the sub-step, e.g., $\bar{\phi}(\mathbf{X}, s) = \bar{\phi}(\mathbf{X}, t_0)$. Hence the scalar mean at t_0 approximated by the initial particle scalar can be used in (5.5) to construct different splitting schemes including second-order accurate schemes. For the nth particle in the ith cell, the scalar mean is approximated as

$$\bar{\phi}^{(n)}(\mathbf{X}_n, s) = \bar{\phi}^{(n)}(\mathbf{X}_n, t_0) \approx \frac{1}{N_i - 1} \sum_{j=1, j \neq n}^{N_i} \phi_j(t_0) \Bigg|_{\mathbf{x}_j \in \left[\mathbf{x}_i - \frac{\Delta\mathbf{x}_i}{2}, \mathbf{x}_i + \frac{\Delta\mathbf{x}_i}{2}\right]}, \tag{5.6}$$

where the particle itself is removed from the cell mean in order to remove the correlation between the particle and the cell mean. This is a first-order approximation in space to $\bar{\phi}^{(n)}(\mathbf{X}_n, t_0)$. A second-order approximation can be constructed by interpolating the cell mean to the particle position. We consider only the time-stepping error in this work, so the simplest approximation method is used to obtain $\bar{\phi}^{(n)}(\mathbf{X}_n, t_0)$. The grid size is specified to be sufficiently small that the spatial discretization error is small compared to the time-stepping error. All the results in Section 6 show the consistent asymptotical behavior of the numerical errors against the time step for the time steps considered, confirming that the spatial discretization error in the test is significantly smaller than the time-stepping error.

Reaction sub-step $\mathbb{R}$**:** The linear reaction sub-step (5.2) is integrated analytically

$$\varphi(t_1) = \mathcal{R}(\phi_0, \Delta t) = R_b + (\phi_0 - R_b) \exp(R_a \Delta t). \tag{5.7}$$

Scalar mean forcing sub-step $\mathbb{S}$**:** The scalar mean forcing sub-step (5.3) is integrated as

$$\varphi(t_1) = \mathcal{S}(\phi_0, \mathbf{X}(r), s, \Delta t) = \phi_0 + S_m(\mathbf{X}(r), s)\Delta t. \tag{5.8}$$

Scalar variance forcing sub-step $\mathbb{V}$**:** In (5.4), if Ω_ν and $\bar{\phi}$ are frozen at some particle position $\mathbf{X}(r)$ and time s, then the analytical solution to the scalar variance forcing sub-step is

$$\varphi(t_1) = \mathcal{V}(\phi_0, \mathbf{X}(r), s, \Delta t) = \bar{\phi}(\mathbf{X}(r), s) + (\phi_0 - \bar{\phi}(\mathbf{X}(r), s)) \exp(\Omega_\nu(\mathbf{X}(r), s)\Delta t). \tag{5.9}$$

For designing different second-order splitting schemes for the scalar equation only, we consider the limit of no particle movement $\mathbf{X}(r) = \mathbf{X}(0)$ (e.g., $\mathbf{D} = 0$ and $b = 0$ in the SDE), and then the scalar equation is an ODE. If the four scalar sub-steps (5.5), (5.7)–(5.9) are advanced in order (e.g., $\mathbb{M}\mathbb{R}\mathbb{S}\mathbb{V}$) with each one taking one full time step once, the result is first-order

accurate (provided that each sub-step is integrated with at least first-order accuracy). Symmetric splitting schemes can be constructed which potentially have second-order accuracy, for example, the scheme denoted $\mathbb{SVMRMVS}$. By this notation, we mean that the processes $\mathbb{S}, \mathbb{V}, \mathbb{M}, \mathbb{R}, \mathbb{M}, \mathbb{V}, \mathbb{S}$ are performed (in that order) with the initial condition for each process being the result of its predecessor. If a process is performed just once (like $\mathbb{R}$ in this example), then it is performed for a time interval Δt. On the other hand, if the process is performed twice (like $\mathbb{S}, \mathbb{V}$, and $\mathbb{M}$ in this example) then it is for a time interval of $\Delta t/2$ each time.

If each sub-step of $\mathbb{SVMRMVS}$ is integrated with second-order accuracy (e.g., by evaluating coefficients at the mid-time of the sub-step), this splitting is called Strang splitting [48] which has overall second-order accuracy. We denote the Strang splitting scheme as $\mathbb{SVMRMVS}$-I, and write down the scheme in Table 1. The Strang splitting needs to evaluate coefficients at $t_{\frac{1}{4}}$ and $t_{\frac{3}{4}}$, and $\mathbf{X}\left(t_{\frac{1}{4}}\right)$ and $\mathbf{X}\left(t_{\frac{3}{4}}\right)$. These particle locations are not computed in the transport sub-step of the most of the splitting schemes discussed in this work. For most schemes, only $\mathbf{X}(t_0)$, and approximations to $\mathbf{X}(t_{\frac{1}{2}})$ and $\mathbf{X}(t_1)$ are available for the construction of the second-order splitting schemes. It is not necessary, however, to have each sub-step of $\mathbb{SVMRMVS}$ integrated with second-order accuracy to construct a second-order splitting scheme. We consider two splitting schemes $\mathbb{SVMRMVS}$-II and $\mathbb{SVMRMVS}$-III (as shown in Table 1) which involve only first-order integration of some sub-steps, e.g., the first half time step of $\mathcal{S}, \mathcal{V}$ and $\mathcal{M}$. The second-order accuracy of the two splitting schemes $\mathbb{SVMRMVS}$-II and $\mathbb{SVMRMVS}$-III can be easily shown for ODEs (by freezing particle position and by showing that the results from $\mathbb{SVMRMVS}$-II and $\mathbb{SVMRMVS}$-III are consistent with those from $\mathbb{SVMRMVS}$-I up to order Δt^2, using Taylor series expansions). The three schemes in Table 1 can be generalized to a class of second-order splitting schemes by evaluating the scalar coefficients at $t = t_{\frac{1}{2}\pm h}$ ($h \in \left[0, \frac{1}{2}\right]$), i.e., evaluating coefficients at $t = t_{\frac{1}{2}-h}$ for the first half steps of $\mathcal{S}, \mathcal{V}$ and $\mathcal{M}$ and at $t = t_{\frac{1}{2}+h}$ for their second half steps. In this work, we only use the splitting $\mathbb{SVMRMVS}$-II and $\mathbb{SVMRMVS}$-III for the construction of the second-order splitting schemes for the coupled SDE system.

The splitting schemes discussed above are applicable to the original scalar Eq. (3.3). They are also applicable to the frozen-coefficient scalar Eq. (3.6) by specifying $s = t_{\frac{1}{2}}$ in function $\mathcal{S}, \mathcal{V}, \mathcal{M}$ (retaining the time r in $\mathbf{X}(r)$ in the schemes).

We can construct different symmetric splitting schemes with potential second-order accuracy, e.g., $\mathbb{SVRMRVS}, \mathbb{MRSVSRM}$. We will not discuss the difference of these different splittings for the scalar equation. In practice, performing one step of reaction $\mathbb{R}$ (like $\mathbb{SVMRMVS}$) in the middle is preferable. Usually, the reaction computation in combustion is dominant, so reducing the number of sub-steps of reactions in the computation reduces the overall computational cost linearly. In order to reduce the reaction computational cost significantly, the *in situ* adaptive tabulation (ISAT) method [49] is often used. Taking a longer time step in ISAT reduces the table size and hence speeds up ISAT. Therefore, performing one step of reaction in the splitting is advantageous.

In the following discussion, we will consider only the splitting $\mathbb{SVMRMVS}$. For simplicity, we denote $\mathbb{SVM}$ as $\mathbb{C}$ and $\mathbb{MVS}$ as $\mathbb{C}'$, and so the splitting simply becomes $\mathbb{CRC}'$.

5.2. Splitting schemes for the coupled SDE system

The numerical schemes for the Ito SDE (3.1) and (3.5) and for the augmented particle scalar Eq. (4.5) have been discussed in Sections 3.3 and 5.1, respectively. Second-order accuracy is achieved for solving the individual equation. In this part, we combine these numerical schemes and develop the weak second-order splitting schemes for the coupled SDE system.

5.2.1. Splitting schemes based on the CP scheme

The splitting schemes in this part (5.2.1) are only appropriate for the mid-point SDE schemes (e.g., the CP scheme (3.7) and (3.8)). The splitting scheme first suggested by Cao and Pope [25] is denoted by $\mathbb{T}_1^{cp}\mathbb{CRC}'\mathbb{T}_2^{cp}$ in Table 2, where the functions $\mathcal{T}_1^{cp}$ and $\mathcal{T}_2^{cp}$ are defined in (3.7) and (3.8), and the splitting scheme $\mathbb{SVMRMVS}$-II in Table 1 is used for the scalar equation. Note that this scheme is not symmetrical, in that the final process $\mathcal{T}_2^{cp}$ is different from the first process $\mathcal{T}_1^{cp}$.

From the previous discussions, if the equations for $\mathbf{X}(t)$ and $\phi(t)$ are integrated separately, $\mathbf{Y}(t_1)$ and $\varphi(t_1)$ from $\mathbb{T}_1^{cp}\mathbb{CRC}'\mathbb{T}_2^{cp}$ are (weak) second-order approximations to $\mathbf{X}(t_1)$ and $\phi(t_1)$, respectively. When coupled, in order to achieve

Table 1
Second-order splitting schemes for the particle scalar Eq. (4.5).

$\mathbb{SVMRMVS}$-I	$\mathbb{SVMRMVS}$-II	$\mathbb{SVMRMVS}$-III
$\varphi_1 = \mathcal{S}\left(\phi_0, \mathbf{X}\left(t_{\frac{1}{4}}\right), t_{\frac{1}{4}}, \frac{\Delta t}{2}\right)$	$\varphi_1 = \mathcal{S}\left(\phi_0, \mathbf{X}\left(t_{\frac{1}{2}}\right), t_{\frac{1}{2}}, \frac{\Delta t}{2}\right)$	$\varphi_1 = \mathcal{S}\left(\phi_0, \mathbf{X}(t_0), t_0, \frac{\Delta t}{2}\right)$
$\varphi_2 = \mathcal{V}\left(\varphi_1, \mathbf{X}\left(t_{\frac{1}{4}}\right), t_{\frac{1}{4}}, \frac{\Delta t}{2}\right)$	$\varphi_2 = \mathcal{V}\left(\varphi_1, \mathbf{X}\left(t_{\frac{1}{2}}\right), t_{\frac{1}{2}}, \frac{\Delta t}{2}\right)$	$\varphi_2 = \mathcal{V}\left(\varphi_1, \mathbf{X}(t_0), t_0, \frac{\Delta t}{2}\right)$
$\varphi_3 = \mathcal{M}\left(\varphi_2, \mathbf{X}\left(t_{\frac{1}{4}}\right), t_{\frac{1}{4}}, \frac{\Delta t}{2}\right)$	$\varphi_3 = \mathcal{M}\left(\varphi_2, \mathbf{X}\left(t_{\frac{1}{2}}\right), t_{\frac{1}{2}}, \frac{\Delta t}{2}\right)$	$\varphi_3 = \mathcal{M}\left(\varphi_2, \mathbf{X}(t_0), t_0, \frac{\Delta t}{2}\right)$
$\varphi_4 = \mathcal{R}(\varphi_3, \Delta t)$	$\varphi_4 = \mathcal{R}(\varphi_3, \Delta t)$	$\varphi_4 = \mathcal{R}(\varphi_3, \Delta t)$
$\varphi_5 = \mathcal{M}\left(\varphi_4, \mathbf{X}\left(t_{\frac{3}{4}}\right), t_{\frac{3}{4}}, \frac{\Delta t}{2}\right)$	$\varphi_5 = \mathcal{M}\left(\varphi_4, \mathbf{X}\left(t_{\frac{1}{2}}\right), t_{\frac{1}{2}}, \frac{\Delta t}{2}\right)$	$\varphi_5 = \mathcal{M}\left(\varphi_4, \mathbf{X}(t_1), t_1, \frac{\Delta t}{2}\right)$
$\varphi_6 = \mathcal{V}\left(\varphi_5, \mathbf{X}\left(t_{\frac{3}{4}}\right), t_{\frac{3}{4}}, \frac{\Delta t}{2}\right)$	$\varphi_6 = \mathcal{V}\left(\varphi_5, \mathbf{X}\left(t_{\frac{1}{2}}\right), t_{\frac{1}{2}}, \frac{\Delta t}{2}\right)$	$\varphi_6 = \mathcal{V}\left(\varphi_5, \mathbf{X}(t_1), t_1, \frac{\Delta t}{2}\right)$
$\varphi(t_1) = \mathcal{S}\left(\varphi_6, \mathbf{X}\left(t_{\frac{3}{4}}\right), t_{\frac{3}{4}}, \frac{\Delta t}{2}\right)$	$\varphi(t_1) = \mathcal{S}\left(\varphi_6, \mathbf{X}\left(t_{\frac{1}{2}}\right), t_{\frac{1}{2}}, \frac{\Delta t}{2}\right)$	$\varphi(t_1) = \mathcal{S}\left(\varphi_6, \mathbf{X}(t_1), t_1, \frac{\Delta t}{2}\right)$

Table 2
Splitting schemes for the coupled SDE system (3.1) (or (3.5)) and (4.5) based on the CP scheme (3.7) and (3.8).

$\mathbb{T}_1^{cp}\mathbb{C}\mathbb{R}\mathbb{C}'\mathbb{T}_2^{cp}$	$\mathbb{T}_1^{cp}\widehat{\mathbb{T}}_1^{cp}\mathbb{C}\mathbb{R}\mathbb{C}'\mathbb{T}_2^{cp}$	$\mathbb{T}_1^{cp}\widehat{\mathbb{T}}_1^{cp}\mathbb{C}\mathbb{R}\mathbb{C}'\mathbb{T}_2^{cp}$-F
	$\mathbf{Y}\left(t_{\frac{1}{2}}\right) = \mathbf{X}_0 + \mathcal{T}_1^{cp}\left(\mathbf{X}_0, t_0, \Delta t, \frac{\xi+\eta}{2} + \frac{\vartheta}{\sqrt{2}}\right)$	$\mathbf{Y}\left(t_{\frac{1}{2}}\right) = \mathbf{X}_0 + \mathcal{T}_1^{cp}\left(\mathbf{X}_0, t_{\frac{1}{2}}, \Delta t, \frac{\xi+\eta}{2} + \frac{\vartheta}{\sqrt{2}}\right)$
$\mathbf{Y}\left(t_{\frac{1}{2}}\right) = \mathbf{X}_0 + \mathcal{T}_1^{cp}(\mathbf{X}_0, t_0, \Delta t, \zeta)$	$\widehat{\mathbf{Y}}\left(t_{\frac{1}{2}}\right) = \mathbf{X}_0 + \mathcal{T}_1^{cp}(\mathbf{X}_0, t_0, \Delta t, \zeta)$	$\widehat{\mathbf{Y}}\left(t_{\frac{1}{2}}\right) = \mathbf{X}_0 + \mathcal{T}_1^{cp}\left(\mathbf{X}_0, t_{\frac{1}{2}}, \Delta t, \zeta\right)$

$$\varphi_1 = \mathcal{S}\left(\phi_0, \mathbf{Y}\left(t_{\frac{1}{2}}\right), t_{\frac{1}{2}}, \frac{\Delta t}{2}\right), \quad \varphi_2 = \mathcal{V}\left(\varphi_1, \mathbf{Y}\left(t_{\frac{1}{2}}\right), t_{\frac{1}{2}}, \frac{\Delta t}{2}\right), \quad \varphi_3 = \mathcal{M}\left(\varphi_2, \mathbf{Y}\left(t_{\frac{1}{2}}\right), t_{\frac{1}{2}}, \frac{\Delta t}{2}\right), \quad \varphi_4 = \mathcal{R}(\varphi_3, \Delta t)$$

$$\varphi_5 = \mathcal{M}\left(\varphi_4, \mathbf{Y}\left(t_{\frac{1}{2}}\right), t_{\frac{1}{2}}, \frac{\Delta t}{2}\right), \quad \varphi_6 = \mathcal{V}\left(\varphi_5, \mathbf{Y}\left(t_{\frac{1}{2}}\right), t_{\frac{1}{2}}, \frac{\Delta t}{2}\right), \quad \varphi(t_1) = \mathcal{S}\left(\varphi_6, \mathbf{Y}\left(t_{\frac{1}{2}}\right), t_{\frac{1}{2}}, \frac{\Delta t}{2}\right)$$

$\mathbf{Y}(t_1) = \mathbf{Y}\left(t_{\frac{1}{2}}\right) + \mathcal{T}_2^{cp}\left(\mathbf{X}_0, \mathbf{Y}\left(t_{\frac{1}{2}}\right), t_{\frac{1}{2}}, \Delta t, \xi, \eta\right)$	$\mathbf{Y}(t_1) = \widehat{\mathbf{Y}}\left(t_{\frac{1}{2}}\right) + \mathcal{T}_2^{cp}\left(\mathbf{X}_0, \widehat{\mathbf{Y}}\left(t_{\frac{1}{2}}\right), t_{\frac{1}{2}}, \Delta t, \xi, \eta\right)$

overall weak second-order accuracy, $\mathbf{Y}\left(t_{\frac{1}{2}}\right)$ must be a weak first-order approximation to the mid-point $\mathbf{X}\left(t_{\frac{1}{2}}\right)$ given the initial and final positions $\mathbf{X}_0$ and $\mathbf{Y}(t_1)$. However, the sub-steps of the CP scheme (3.7) and (3.8) use independent Gaussian random vectors, which makes the mid-point approximation $\mathbf{Y}\left(t_{\frac{1}{2}}\right)$ impossible to represent the correct distribution given the initial and final positions. Hence the splitting scheme $\mathbb{T}_1^{cp}\mathbb{C}\mathbb{R}\mathbb{C}'\mathbb{T}_2^{cp}$ degrades to overall first-order accuracy despite of the second-order accuracy achieved by each equation.

Introducing another mid-point $\mathbf{Y}\left(t_{\frac{1}{2}}\right)$ (the original one is $\widehat{\mathbf{Y}}\left(t_{\frac{1}{2}}\right)$) which is correlated to the increment of the second-step of the CP scheme achieves overall second-order accuracy. The new splitting scheme is shown as $\mathbb{T}_1^{cp}\widehat{\mathbb{T}}_1^{cp}\mathbb{C}\mathbb{R}\mathbb{C}'\mathbb{T}_2^{cp}$ in Table 2 in which the $\widehat{\mathbf{Y}}\left(t_{\frac{1}{2}}\right)$ step is denoted by $\widehat{\mathbb{T}}_1^{cp}$, and ϑ is another independent Gaussian random vector. The step $\mathbb{T}_1^{cp}$ is exactly the same as $\widehat{\mathbb{T}}_1^{cp}$ except using a different random vector for the Wiener process. The second-step (3.8) of the CP scheme can be simply viewed as a Wiener process $\mathbf{W}(t)$. If we consider $\mathbf{W}(t_1) = \xi + \eta$ at $t_1 = 2$ starting from $\mathbf{W}(t_0) = 0$, then $\mathbf{W}\left(t_{\frac{1}{2}}\right)$ has the same distribution as $\frac{\xi+\eta}{2} + \frac{\vartheta}{\sqrt{2}}$. Therefore, $\mathbf{Y}\left(t_{\frac{1}{2}}\right)$ represents the distribution of $\mathbf{X}\left(t_{\frac{1}{2}}\right)$ correctly, and this splitting scheme $\mathbb{T}_1^{cp}\widehat{\mathbb{T}}_1^{cp}\mathbb{C}\mathbb{R}\mathbb{C}'\mathbb{T}_2^{cp}$ is expected to be overall second-order accurate. The results below confirm this expectation.

We can apply the second-order splitting $\mathbb{T}_1^{cp}\widehat{\mathbb{T}}_1^{cp}\mathbb{C}\mathbb{R}\mathbb{C}'\mathbb{T}_2^{cp}$ to the frozen-coefficient SDE system (3.5) and (3.6), and obtain the scheme $\mathbb{T}_1^{cp}\widehat{\mathbb{T}}_1^{cp}\mathbb{C}\mathbb{R}\mathbb{C}'\mathbb{T}_2^{cp}$-F in Table 2 where "F" denotes the frozen-coefficient system.

The schemes in Table 2 (in standard form) are not symmetric, whereas those below are.

5.2.2. Splitting schemes of type $\mathbb{T}\mathbb{C}\mathbb{R}\mathbb{C}'\mathbb{T}$

Second-order splitting schemes can be constructed based on any Ito SDE schemes (e.g., the KP scheme and the TV scheme in Section 3.3). We can construct the scheme of the type $\mathbb{T}\mathbb{C}\mathbb{R}\mathbb{C}'\mathbb{T}$. The splitting with the CP scheme is written as $\mathbb{T}^{cp}\mathbb{C}\mathbb{R}\mathbb{C}'\mathbb{T}^{cp}$ in Table 3 where $\mathcal{T}^{cp}$ is defined in (3.10). In contrast to the CP schemes described in previous sub-sections, this scheme performs a complete CP step (of duration $\Delta t/2$) on each of the first and last sub-steps. Similarly, we can construct the splitting schemes with the TV scheme $\mathbb{T}^{tv}\mathbb{C}\mathbb{R}\mathbb{C}'\mathbb{T}^{tv}$ in Table 3 with $\mathcal{T}^{tv}$ defined in (3.14).

Applying the splitting scheme to the frozen-coefficient SDE system with CP and TV schemes, we have the $\mathbb{T}^{cp}\mathbb{C}\mathbb{R}\mathbb{C}'\mathbb{T}^{cp}$-F scheme and the $\mathbb{T}^{tv}\mathbb{C}\mathbb{R}\mathbb{C}'\mathbb{T}^{tv}$-F scheme as shown in Table 4. The KP scheme is only applicable to the frozen-coefficient system, so the splitting scheme combining the KP scheme is $\mathbb{T}^{kp}\mathbb{C}\mathbb{R}\mathbb{C}'\mathbb{T}^{kp}$-F in Table 4 with $\mathcal{T}^{kp}$ defined in (3.12).

We discussed five splitting schemes of the type of $\mathbb{T}\mathbb{C}\mathbb{R}\mathbb{C}'\mathbb{T}$, which are all confirmed to be second-order accurate by the results below.

5.2.3. Splitting schemes of type $\mathbb{C}\mathbb{T}\mathbb{R}\mathbb{T}\mathbb{C}'$

We can design other second-order splitting schemes using different combinations of the transport sub-step and scalar sub-step. One example is $\mathbb{C}\mathbb{T}\mathbb{R}\mathbb{T}\mathbb{C}'$, which takes one step of reaction with half steps of transport right before and after the reaction sub-step. As expected, this splitting scheme is second-order accurate. This splitting combined with the CP and TV schemes are denoted by $\mathbb{C}\mathbb{T}^{cp}\mathbb{R}\mathbb{T}^{cp}\mathbb{C}'$ and $\mathbb{C}\mathbb{T}^{tv}\mathbb{R}\mathbb{T}^{tv}\mathbb{C}'$, respectively, in Table 5 where the splitting scheme $\mathbb{S}\mathbb{V}\mathbb{M}\mathbb{R}\mathbb{M}\mathbb{V}\mathbb{S}$-III in

Table 3
Splitting schemes of the type $\mathbb{T}\mathbb{C}\mathbb{R}\mathbb{C}'\mathbb{T}$ for the coupled SDE system (3.1) and (4.5).

$\mathbb{T}^{cp}\mathbb{C}\mathbb{R}\mathbb{C}'\mathbb{T}^{cp}$	$\mathbb{T}^{tv}\mathbb{C}\mathbb{R}\mathbb{C}'\mathbb{T}^{tv}$
$\mathbf{Y}\left(t_{\frac{1}{2}}\right) = \mathbf{X}_0 + \mathcal{T}^{cp}\left(\mathbf{X}_0, t_0, t_{\frac{1}{4}}, \frac{\Delta t}{2}, \zeta, \xi, \eta\right)$	$Y\left(t_{\frac{1}{2}}\right) = X_0 + \mathcal{T}^{tv}\left(X_0, \frac{\Delta t}{2}, t_0, \mu_0, \bar{\mu}_0, \xi\right)$

$$\varphi_1 = \mathcal{S}\left(\phi_0, \mathbf{Y}\left(t_{\frac{1}{2}}\right), t_{\frac{1}{2}}, \frac{\Delta t}{2}\right), \quad \varphi_2 = \mathcal{V}\left(\varphi_1, \mathbf{Y}\left(t_{\frac{1}{2}}\right), t_{\frac{1}{2}}, \frac{\Delta t}{2}\right), \quad \varphi_3 = \mathcal{M}\left(\varphi_2, \mathbf{Y}(t_{\frac{1}{2}}), t_{\frac{1}{2}}, \frac{\Delta t}{2}\right), \quad \varphi_4 = \mathcal{R}(\varphi_3, \Delta t)$$

$$\varphi_5 = \mathcal{M}\left(\varphi_4, \mathbf{Y}\left(t_{\frac{1}{2}}\right), t_{\frac{1}{2}}, \frac{\Delta t}{2}\right), \quad \varphi_6 = \mathcal{V}\left(\varphi_5, \mathbf{Y}\left(t_{\frac{1}{2}}\right), t_{\frac{1}{2}}, \frac{\Delta t}{2}\right), \quad \varphi(t_1) = \mathcal{S}\left(\varphi_6, \mathbf{Y}\left(t_{\frac{1}{2}}\right), t_{\frac{1}{2}}, \frac{\Delta t}{2}\right)$$

$\mathbf{Y}(t_1) = \mathbf{Y}\left(t_{\frac{1}{2}}\right) + \mathcal{T}^{cp}\left(\mathbf{Y}\left(t_{\frac{1}{2}}\right), t_{\frac{1}{2}}, t_{\frac{3}{4}}, \frac{\Delta t}{2}, \zeta', \xi', \eta'\right)$	$Y(t_1) = Y\left(t_{\frac{1}{2}}\right) + \mathcal{T}^{tv}\left(Y\left(t_{\frac{1}{2}}\right), \frac{\Delta t}{2}, t_{\frac{1}{2}}, \mu_0, \bar{\mu}_0, \xi'\right)$

Table 4
Splitting schemes of the type $\mathbb{T}\mathbb{C}\mathbb{R}\mathbb{C}'\mathbb{T}$ for the coupled SDE system (3.5) and (4.5).

$\mathbb{T}^{cp}\mathbb{C}\mathbb{R}\mathbb{C}'\mathbb{T}^{cp}$-F	$\mathbb{T}^{tv}\mathbb{C}\mathbb{R}\mathbb{C}'\mathbb{T}^{tv}$-F	$\mathbb{T}^{kp}\mathbb{C}\mathbb{R}\mathbb{C}'\mathbb{T}^{kp}$-F
$\mathbf{Y}\left(t_{\frac{1}{2}}\right) = \mathbf{X}_0 + \mathcal{T}^{cp}\left(\mathbf{X}_0, t_{\frac{1}{2}}, t_{\frac{1}{2}}, \frac{\Delta t}{2}, \zeta, \xi, \eta\right)$	$Y\left(t_{\frac{1}{2}}\right) = X_0 + \mathcal{T}^{tv}\left(X_0, \frac{\Delta t}{2}, t_{\frac{1}{2}}, 0, 0, \xi\right)$	$Y\left(t_{\frac{1}{2}}\right) = X_0 + \mathcal{T}^{kp}(X_0, \frac{\Delta t}{2}, \xi)$

$$\varphi_1 = \mathcal{S}\left(\phi_0, \mathbf{Y}\left(t_{\frac{1}{2}}\right), t_{\frac{1}{2}}, \frac{\Delta t}{2}\right), \quad \varphi_2 = \mathcal{V}\left(\varphi_1, \mathbf{Y}\left(t_{\frac{1}{2}}\right), t_{\frac{1}{2}}, \frac{\Delta t}{2}\right), \quad \varphi_3 = \mathcal{M}\left(\varphi_2, \mathbf{Y}(t_{\frac{1}{2}}), t_{\frac{1}{2}}, \frac{\Delta t}{2}\right), \quad \varphi_4 = \mathcal{R}(\varphi_3, \Delta t)$$

$$\varphi_5 = \mathcal{M}\left(\varphi_4, \mathbf{Y}\left(t_{\frac{1}{2}}\right), t_{\frac{1}{2}}, \frac{\Delta t}{2}\right), \quad \varphi_6 = \mathcal{V}\left(\varphi_5, \mathbf{Y}\left(t_{\frac{1}{2}}\right), t_{\frac{1}{2}}, \frac{\Delta t}{2}\right), \quad \varphi(t_1) = \mathcal{S}\left(\varphi_6, \mathbf{Y}\left(t_{\frac{1}{2}}\right), t_{\frac{1}{2}}, \frac{\Delta t}{2}\right)$$

| $\mathbf{Y}(t_1) = \mathbf{Y}\left(t_{\frac{1}{2}}\right) + \mathcal{T}^{cp}\left(\mathbf{Y}\left(t_{\frac{1}{2}}\right), t_{\frac{1}{2}}, t_{\frac{1}{2}}, \frac{\Delta t}{2}, \zeta', \xi', \eta'\right)$ | $Y(t_1) = Y\left(t_{\frac{1}{2}}\right) + \mathcal{T}^{tv}\left(Y\left(t_{\frac{1}{2}}\right), \frac{\Delta t}{2}, t_{\frac{1}{2}}, 0, 0, \xi'\right)$ | $Y(t_1) = Y\left(t_{\frac{1}{2}}\right) + \mathcal{T}^{kp}\left(Y\left(t_{\frac{1}{2}}\right), \frac{\Delta t}{2}, \xi'\right)$ |

Table 5
Splitting schemes of the type $\mathbb{C}\mathbb{T}\mathbb{R}\mathbb{T}\mathbb{C}'$ for the coupled SDE system (3.1) and (4.5).

$\mathbb{C}\mathbb{T}^{cp}\mathbb{R}\mathbb{T}^{cp}\mathbb{C}'$	$\mathbb{C}\mathbb{T}^{tv}\mathbb{R}\mathbb{T}^{tv}\mathbb{C}'$

$$\varphi_1 = \mathcal{S}(\phi_0, \mathbf{X}_0, t_0, \frac{\Delta t}{2}), \quad \varphi_2 = \mathcal{V}(\varphi_1, \mathbf{X}_0, t_0, \frac{\Delta t}{2}), \quad \varphi_3 = \mathcal{M}(\varphi_2, \mathbf{X}_0, t_0, \frac{\Delta t}{2})$$

| $\mathbf{Y}\left(t_{\frac{1}{2}}\right) = \mathbf{X}_0 + \mathcal{T}^{cp}\left(\mathbf{X}_0, t_0, t_{\frac{1}{4}}, \frac{\Delta t}{2}, \zeta, \xi, \eta\right)$ | $Y\left(t_{\frac{1}{2}}\right) = X_0 + \mathcal{T}^{tv}(X_0, \frac{\Delta t}{2}, t_0, \mu_0, \bar{\mu}_0, \xi)$ |

$$\varphi_4 = \mathcal{R}(\varphi_3, \Delta t)$$

| $\mathbf{Y}(t_1) = \mathbf{Y}\left(t_{\frac{1}{2}}\right) + \mathcal{T}^{cp}\left(\mathbf{Y}\left(t_{\frac{1}{2}}\right), t_{\frac{1}{2}}, t_{\frac{3}{4}}, \frac{\Delta t}{2}, \zeta', \xi', \eta'\right)$ | $Y(t_1) = Y\left(t_{\frac{1}{2}}\right) + \mathcal{T}^{tv}\left(Y\left(t_{\frac{1}{2}}\right), \frac{\Delta t}{2}, t_{\frac{1}{2}}, \mu_0, \bar{\mu}_0, \xi'\right)$ |

$$\varphi_5 = \mathcal{M}(\varphi_4, \mathbf{Y}(t_1), t_1, \frac{\Delta t}{2}), \quad \varphi_6 = \mathcal{V}(\varphi_5, \mathbf{Y}(t_1), t_1, \frac{\Delta t}{2}), \quad \varphi(t_1) = \mathcal{S}(\varphi_6, \mathbf{Y}(t_1), t_1, \frac{\Delta t}{2})$$

Table 6
Splitting schemes of the type $\mathbb{C}\mathbb{T}\mathbb{R}\mathbb{T}\mathbb{C}'$ for the coupled SDE system (3.5) and (4.5).

$\mathbb{C}\mathbb{T}^{cp}\mathbb{R}\mathbb{T}^{cp}\mathbb{C}' - F$	$\mathbb{C}\mathbb{T}^{tv}\mathbb{R}\mathbb{T}^{tv}\mathbb{C}'$-F	$\mathbb{C}\mathbb{T}^{kp}\mathbb{R}\mathbb{T}^{kp}\mathbb{C}'$-F

$$\varphi_1 = \mathcal{S}\left(\phi_0, \mathbf{X}_0, t_{\frac{1}{2}}, \frac{\Delta t}{2}\right), \quad \varphi_2 = \mathcal{V}\left(\varphi_1, \mathbf{X}_0, t_{\frac{1}{2}}, \frac{\Delta t}{2}\right), \quad \varphi_3 = \mathcal{M}\left(\varphi_2, \mathbf{X}_0, t_{\frac{1}{2}}, \frac{\Delta t}{2}\right)$$

$\mathbf{Y}\left(t_{\frac{1}{2}}\right) = \mathbf{X}_0 + \mathcal{T}^{cp}\left(\mathbf{X}_0, t_{\frac{1}{2}}, t_{\frac{1}{2}}, \frac{\Delta t}{2}, \zeta, \xi, \eta\right)$	$Y\left(t_{\frac{1}{2}}\right) = X_0 + \mathcal{T}^{tv}\left(X_0, \frac{\Delta t}{2}, t_{\frac{1}{2}}, 0, 0, \xi\right)$	$Y\left(t_{\frac{1}{2}}\right) = X_0 + \mathcal{T}^{kp}(X_0, \frac{\Delta t}{2}, \xi)$
	$\varphi_4 = \mathcal{R}(\varphi_3, \Delta t)$	
$\mathbf{Y}(t_1) = \mathbf{Y}\left(t_{\frac{1}{2}}\right) + \mathcal{T}^{cp}\left(\mathbf{Y}\left(t_{\frac{1}{2}}\right), t_{\frac{1}{2}}, t_{\frac{1}{2}}, \frac{\Delta t}{2}, \zeta', \xi', \eta'\right)$	$Y(t_1) = Y\left(t_{\frac{1}{2}}\right) + \mathcal{T}^{tv}\left(Y\left(t_{\frac{1}{2}}\right), \frac{\Delta t}{2}, t_{\frac{1}{2}}, 0, 0, \xi'\right)$	$Y(t_1) = Y\left(t_{\frac{1}{2}}\right) + \mathcal{T}^{kp}\left(Y\left(t_{\frac{1}{2}}\right), \frac{\Delta t}{2}, \xi'\right)$

$$\varphi_5 = \mathcal{M}\left(\varphi_4, \mathbf{Y}(t_1), t_{\frac{1}{2}}, \frac{\Delta t}{2}\right), \quad \varphi_6 = \mathcal{V}\left(\varphi_5, \mathbf{Y}(t_1), t_{\frac{1}{2}}, \frac{\Delta t}{2}\right), \quad \varphi(t_1) = \mathcal{S}\left(\varphi_6, \mathbf{Y}(t_1), t_{\frac{1}{2}}, \frac{\Delta t}{2}\right)$$

Table 1 for the scalar equation is used. The splitting $\mathbb{C}\mathbb{T}\mathbb{R}\mathbb{T}\mathbb{C}'$ combined with the CP, TV and KP schemes for the frozen-coefficient system (3.5) and (3.6) are denoted by $\mathbb{C}\mathbb{T}^{cp}\mathbb{R}\mathbb{T}^{cp}\mathbb{C}'$-F, $\mathbb{C}\mathbb{T}^{tv}\mathbb{R}\mathbb{T}^{tv}\mathbb{C}'$-F and $\mathbb{C}\mathbb{T}^{kp}\mathbb{R}\mathbb{T}^{kp}\mathbb{C}'$-F in Table 6.

Five second-order splitting schemes of the type of $\mathbb{C}\mathbb{T}\mathbb{R}\mathbb{T}\mathbb{C}'$ are discussed in this part 5.2.3. Second-order accuracy of these schemes are confirmed by the results below.

5.2.4. Splitting schemes of type $\mathbb{C}\mathbb{R}\mathbb{T}\mathbb{C}'$

In this work, the restriction of constant density has been made for the discussion, which makes the transport sub-step independent of the reaction sub-step, so that the transport sub-step $\mathbb{T}$ and the reaction sub-step $\mathbb{R}$ can be commuted if they are adjacent to each other in a splitting scheme. The previous splitting $\mathbb{C}\mathbb{T}\mathbb{R}\mathbb{T}\mathbb{C}'$ is the same as $\mathbb{C}\mathbb{R}\mathbb{T}\mathbb{T}\mathbb{C}'$ (i.e., with $\mathbb{T}$ and $\mathbb{R}$ commuted). The two $\mathbb{T}$ sub-steps can be combined to yield $\mathbb{C}\mathbb{R}\mathbb{T}\mathbb{C}'$. (It should be noticed that $\mathbb{C}\mathbb{T}\mathbb{R}\mathbb{T}\mathbb{C}'$ is identical to $\mathbb{C}\mathbb{R}\mathbb{T}\mathbb{T}\mathbb{C}'$, but that $\mathbb{T}$ is not identical to $\mathbb{T}\mathbb{T}$: they both do a second-order step of size Δt, but with different truncation error.) This scheme $\mathbb{C}\mathbb{R}\mathbb{T}\mathbb{C}'$ requires only one step of reaction and one step of transport, and it is second-order accurate for constant-density problems. This splitting combined with the CP scheme and TV schemes are denoted by $\mathbb{C}\mathbb{R}\mathbb{T}^{cp}\mathbb{C}'$ and $\mathbb{C}\mathbb{R}\mathbb{T}^{tv}\mathbb{C}'$ in

Table 7
Splitting schemes of the type $\mathbb{C}\mathbb{R}\mathbb{T}\mathbb{C}'$ for the coupled SDE system (3.1) and (4.5).

$\mathbb{C}\mathbb{R}\mathbb{T}^{cp}\mathbb{C}'$	$\mathbb{C}\mathbb{R}\mathbb{T}^{tv}\mathbb{C}'$

$$\varphi_1 = \mathcal{S}(\phi_0, \mathbf{X}_0, t_0, \frac{\Delta t}{2}), \quad \varphi_2 = \mathcal{V}(\varphi_1, \mathbf{X}_0, t_0, \frac{\Delta t}{2}), \quad \varphi_3 = \mathcal{M}(\varphi_2, \mathbf{X}_0, t_0, \frac{\Delta t}{2})$$
$$\varphi_4 = \mathcal{R}(\varphi_3, \Delta t)$$

| $\mathbf{Y}(t_1) = \mathbf{X}_0 + \mathcal{T}^{cp}\left(\mathbf{X}_0, t_0, t_{\frac{1}{2}}, \Delta t, \zeta, \xi, \eta\right)$ | $Y(t_1) = X_0 + \mathcal{T}^{tv}(X_0, \Delta t, t_0, \mu_0, \bar{\mu}_0, \xi)$ |

$$\varphi_5 = \mathcal{M}(\varphi_4, \mathbf{Y}(t_1), t_1, \frac{\Delta t}{2}), \quad \varphi_6 = \mathcal{V}(\varphi_5, \mathbf{Y}(t_1), t_1, \frac{\Delta t}{2}), \quad \varphi(t_1) = \mathcal{S}(\varphi_6, \mathbf{Y}(t_1), t_1, \frac{\Delta t}{2})$$

Table 8
Splitting schemes of the type $\mathbb{CRTC}'$ for the coupled SDE system (3.5) and (4.5).

$\mathbb{CRT}^{cp}\mathbb{C}' - \mathbf{F}$	$\mathbb{CRT}^{tv}\mathbb{C}' - \mathbf{F}$	$\mathbb{CRT}^{kp}\mathbb{C}'$-$\mathbf{F}$
$\varphi_1 = \mathcal{S}\left(\phi_0, \mathbf{X}_0, t_{\frac{1}{2}}, \frac{\Delta t}{2}\right)$, $\quad \varphi_2 = \mathcal{V}\left(\varphi_1, \mathbf{X}_0, t_{\frac{1}{2}}, \frac{\Delta t}{2}\right)$, $\quad \varphi_3 = \mathcal{M}\left(\varphi_2, \mathbf{X}_0, t_{\frac{1}{2}}, \frac{\Delta t}{2}\right)$, $\quad \varphi_4 = \mathcal{R}(\varphi_3, \Delta t)$		
$\mathbf{Y}(t_1) = \mathbf{X}_0 + \mathcal{T}^{cp}\left(\mathbf{X}_0, t_{\frac{1}{2}}, t_{\frac{1}{2}}, \Delta t, \zeta, \xi, \boldsymbol{\eta}\right)$	$Y(t_1) = X_0 + \mathcal{T}^{tv}\left(X_0, \Delta t, t_{\frac{1}{2}}, 0, \xi\right)$	$Y(t_1) = X_0 + \mathcal{T}^{kp}(X_0, \Delta t, \xi)$
$\varphi_5 = \mathcal{M}\left(\varphi_4, \mathbf{Y}(t_1), t_{\frac{1}{2}}, \frac{\Delta t}{2}\right)$, $\quad \varphi_6 = \mathcal{V}\left(\varphi_5, \mathbf{Y}(t_1), t_{\frac{1}{2}}, \frac{\Delta t}{2}\right)$, $\quad \varphi(t_1) = \mathcal{S}\left(\varphi_6, \mathbf{Y}(t_1), t_{\frac{1}{2}}, \frac{\Delta t}{2}\right)$		

Table 7. When used on the frozen-coefficient system (3.5) and (3.6), the splitting yields $\mathbb{CRT}^{cp}\mathbb{C}'$-F,$\mathbb{CRT}^{tv}\mathbb{C}'$-F and $\mathbb{CRT}^{\,kp}\mathbb{C}'$-F as shown in Table 8 when combined with the CP, TV and KP schemes.

Five second-order splitting schemes of the type $\mathbb{CRTC}'$ are discussed in this part 5.2.4, and their second-order accuracy is confirmed in Section 6.

In summary, in this section, we developed the sub-stepping scheme of the scalar evolution (4.5) and different splitting schemes for the stochastic particle equations. There are certainly many other second-order splitting schemes not discussed above. We limit our discussion on the above proposed splitting schemes. In the next section, we report convergence tests which confirm the order of accuracy of the proposed splitting schemes. The testing and discussion can be applied to other splitting schemes not discussed in this paper (such as $\mathbb{TSVRMRVST}$ or $\mathbb{SVTMRMTVS}$).

6. Convergence tests

The convergence tests are performed for a one-dimensional periodic turbulent reactive flow system with constant density $(\nabla \cdot \bar{\mathbf{u}} = 0)$. The manufactured solutions to the scalar mean and variance are shown in Appendix C together with the velocity, diffusivity, scalar frequency and forcing terms. For the convergence test of third and fourth moments, we estimate the exact solution of the moments required for evaluating the numerical error from a high-resolution finite-difference solution of the transport equations of these moments (Section 6.3).

The domain $[0, L_0]$ is partitioned into $N_g = 50$ uniform grid cells. The grid is used to calculate the ensemble average of particles for the error estimate (4.8) and to compute the scalar mean (5.6) used in the mixing sub-step (5.5) and in the scalar variance forcing sub-step (5.9). The test case is integrated on $t \in [0, T]$, and $N_t = [1, 2, 4, 6, 8, 10, 12, 16, 20, 24, 32, 40]$ equal time steps (of size $\Delta t = T/N_t$) are taken to the same stopping time T, in order to show the asymptotic convergence with respect to the time step, Δt. In total $N = 50,000$ particles are used for each simulation trial. Independent trails are performed to compute the global error $\mathcal{E}_{\overline{\phi^q}}$ in (B.9). A total of 30 sets of trails are performed to estimate the mean and variance of $\mathcal{E}_{\overline{\phi^q}}$, and hence to construct the 95% confidence interval of the estimated global error. The 95% confidence interval of the global error is $\left[E(\mathcal{E}_{\overline{\phi^q}}) - 1.96 \times \text{std}(\mathcal{E}_{\overline{\phi^q}}), E(\mathcal{E}_{\overline{\phi^q}}) + 1.96 \times \text{std}(\mathcal{E}_{\overline{\phi^q}})\right]$, where "std" is the standard deviation. The confidence interval needs to be small for us to draw confident conclusions. The size of the confidence interval depends on the number of independent trials performed. We require that

$$\frac{1.96 \times \text{std}(\mathcal{E}_{\overline{\phi^q}})}{E(\mathcal{E}_{\overline{\phi^q}})} \leqslant \varepsilon, \tag{6.1}$$

for the moments of the scalar to control the size of the confidence interval, where the threshold ε is increased from 0.1 to 0.95 gradually with decreasing Δt. This requirement is used as a stopping criterion for the simulations. More and more trials are performed and added into the ensemble of trials to estimate the global error until the criterion (6.1) is fulfilled. In the tests, depending on different splitting schemes, up to 1.4×10^6 trials may be required to fulfill the criterion (6.1), resulting effectively in 7×10^{10} particles in total. This kind of simulation can be perfectly performed via parallel computers with little message communication. The simulations are done using 32-processes per case on an HPC cluster of 36 Dell servers featuring dual, dual-core Intel Xeon "Woodcrest" processors, tied together using a QLogic 4X SDR InfiniBand interconnect. The total cost of the convergence test for one splitting scheme is up to 600 CPU-hours for the most expensive case.

The particle positions are initialized to be uniformly distributed in the domain $[0, L_0]$. For the divergence-free flow considered, this uniform spatial distribution remains uniform for all later times (in expectation and absent numerical errors) [1], which guarantees approximately the same number of particles to evaluate the volume average of the scalar moments in (4.7). The periodic boundary condition is applied to the particle position so that all the particles remain in the computational domain at all time. The particle scalar is specified to be Gaussian randomly distributed initially, and is initialized according to the scalar mean $\bar{\phi}_m$ and variance $\overline{\phi'^2}_m$, i.e., $\phi = \bar{\phi}_m + (\overline{\phi'^2}_m)^{\frac{1}{2}}\xi$, where ξ is a standardized Gaussian random number and $\bar{\phi}_m$ and $\overline{\phi'^2}_m$ are evaluated at the particle initial position according to (C.1) and (C.2).

6.1. Order of weak convergence of different splitting schemes

For various CP schemes, Fig. 2 shows the global errors $\mathcal{E}_{\overline{\phi^q}}$ (B.9) of the first moment $\bar{\phi}$ and second moment $\overline{\phi^2}$ against the time step Δt. On these log–log plots, lines of slope one and two indicate first and second-order convergence, respectively. The global errors of all simulations show asymptotic convergence given the 95% confidence interval when Δt decreases to zero.

In Fig. 2, the results of the $\mathbb{T}_1^{cp}\mathbb{C}\mathbb{R}\mathbb{C}'\mathbb{T}_2^{cp}$ scheme (in Table 2) (circles in the figure) show first-order asymptotic behavior in comparison with the reference dash-lines of slope one and two. So this scheme is only first-order accurate for the reason explained in Section 5.2.1. Notice that these results (circles) are obtained using the MMS solutions and forcing terms. These forcing terms do not appear in a realistic problem. To show the effect of these forcing terms, we perform the computations of the same problem (e.g., the same configuration, the same initial and boundary conditions) without the forcing terms. The "exact" solution required for the error measurement (4.8) is obtained from a high-resolution finite-difference simulation. The results (shown as squares in Fig. 2) show first-order convergence, which confirms the first-order accuracy of the $\mathbb{T}_1^{cp}\mathbb{C}\mathbb{R}\mathbb{C}'\mathbb{T}_2^{cp}$ scheme. The numerical errors with MMS terms are about two orders of magnitude larger than without in Fig. 2. This significant difference is caused by the different solutions of the first and second moments at the stopping time with and without MMS terms. As shown in Fig. 3, given the same initial condition and other functions, the profiles of the first and second moments of the scalar with MMS terms are over one order of magnitude larger than those without.

Although the accurate numerical solutions can be obtained for the current verification test case without MMS terms, the MMS is preferable to the accurate numerical solutions in general for the Monte Carlo method. The MMS introduces more processes (forcing terms), which incur more numerical error in the numerical solutions, and hence makes the verification easier in terms of computational cost. Without the MMS terms, the existing test cases indicate that the computational cost may be two orders of magnitude greater than those with MMS terms. In designing the MMS solutions, we need to make sure that none of the terms in the transport equations of scalar mean and variance dominate over the other terms. The magnitudes of the terms for the current test case are examined in Appendix C.

The modified mid-point scheme $\mathbb{T}_1^{cp}\widehat{\mathbb{T}}_1^{cp}\mathbb{C}\mathbb{R}\mathbb{C}'\mathbb{T}_2^{cp}$ in Table 2 improves the convergence rate to second-order as shown by the diamonds in Fig. 2. When the frozen-coefficient SDE system (3.5) and (3.6) is used, the scheme $\mathbb{T}_1^{cp}\widehat{\mathbb{T}}_1^{cp}\mathbb{C}\mathbb{R}\mathbb{C}'\mathbb{T}_2^{cp}$-F retains the same order of accuracy (shown by the down triangles in the figure). Meanwhile, for the test case, it suggests that the absolute error from $\mathbb{T}_1^{cp}\widehat{\mathbb{T}}_1^{cp}\mathbb{C}\mathbb{R}\mathbb{C}'\mathbb{T}_2^{cp}$-F is lower than that from $\mathbb{T}_1^{cp}\widehat{\mathbb{T}}_1^{cp}\mathbb{C}\mathbb{R}\mathbb{C}'\mathbb{T}_2^{cp}$. For schemes $\mathbb{T}_1^{cp}\widehat{\mathbb{T}}_1^{cp}\mathbb{C}\mathbb{R}\mathbb{C}'\mathbb{T}_2^{cp}$ and $\mathbb{T}_1^{cp}\widehat{\mathbb{T}}_1^{cp}\mathbb{C}\mathbb{R}\mathbb{C}'\mathbb{T}_2^{cp}$-F, the required time steps are in the ratio of 1:1.6 for 1% accuracy of the first scalar moment, and in the ratio of 1:1.3 for 1% accuracy of the second scalar moment.

Fig. 4 shows the convergence test results of the five splitting schemes of the type $\mathbb{T}\mathbb{C}\mathbb{R}\mathbb{C}'\mathbb{T}$ described in Section 5.2.2. The convergence results verify the second-order accuracy of the splitting schemes ($\mathbb{T}^{cp}\mathbb{C}\mathbb{R}\mathbb{C}'\mathbb{T}^{cp}$ in Table 3 (circles in Fig. 4), $\mathbb{T}^{tv}\mathbb{C}\mathbb{R}\mathbb{C}'\mathbb{T}^{tv}$ in Table 3 (diamonds in Fig. 4), $\mathbb{T}^{cp}\mathbb{C}\mathbb{R}\mathbb{C}'\mathbb{T}^{cp}$-F in Table 4 (down triangles in Fig. 4), $\mathbb{T}^{tv}\mathbb{C}\mathbb{R}\mathbb{C}'\mathbb{T}^{tv}$-F in Table 4 (left triangles in Fig. 4), $\mathbb{T}^{kp}\mathbb{C}\mathbb{R}\mathbb{C}'\mathbb{T}^{kp}$-F in Table 4 (up triangles in Fig. 4)), and the weak second-order accuracy of the two
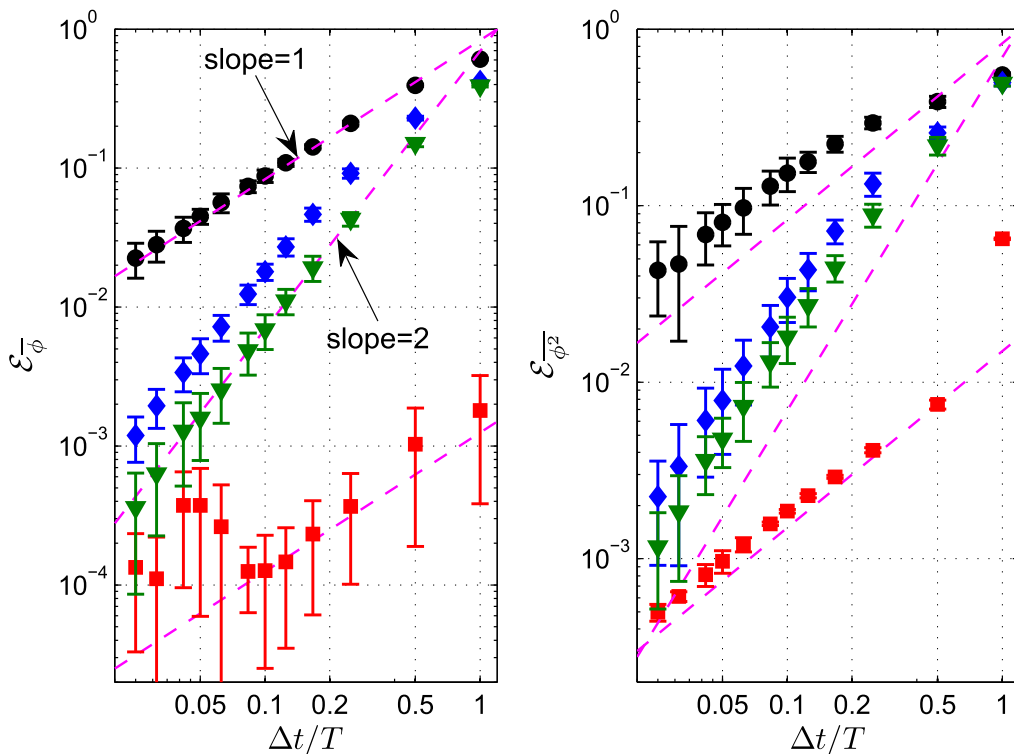

Fig. 2. The convergence of the global error of $\bar{\phi}$ and $\overline{\phi^2}$ against the time step Δt with $\mathbb{T}_1^{cp}\mathbb{C}\mathbb{R}\mathbb{C}'\mathbb{T}_2^{cp}$ in Table 2 (circle), with $\mathbb{T}_1^{cp}\widehat{\mathbb{T}}_1^{cp}\mathbb{C}\mathbb{R}\mathbb{C}'\mathbb{T}_2^{cp}$ in Table 2 (diamond), with $\mathbb{T}_1^{cp}\widehat{\mathbb{T}}_1^{cp}\mathbb{C}\mathbb{R}\mathbb{C}'\mathbb{T}_2^{cp}$-F in Table 2 (down triangle), and with $\mathbb{T}_1^{cp}\mathbb{C}\mathbb{R}\mathbb{C}'\mathbb{T}_2^{cp}$ in Table 2 without MMS forcing terms (square). (The error bars indicate 95% confidence intervals.)
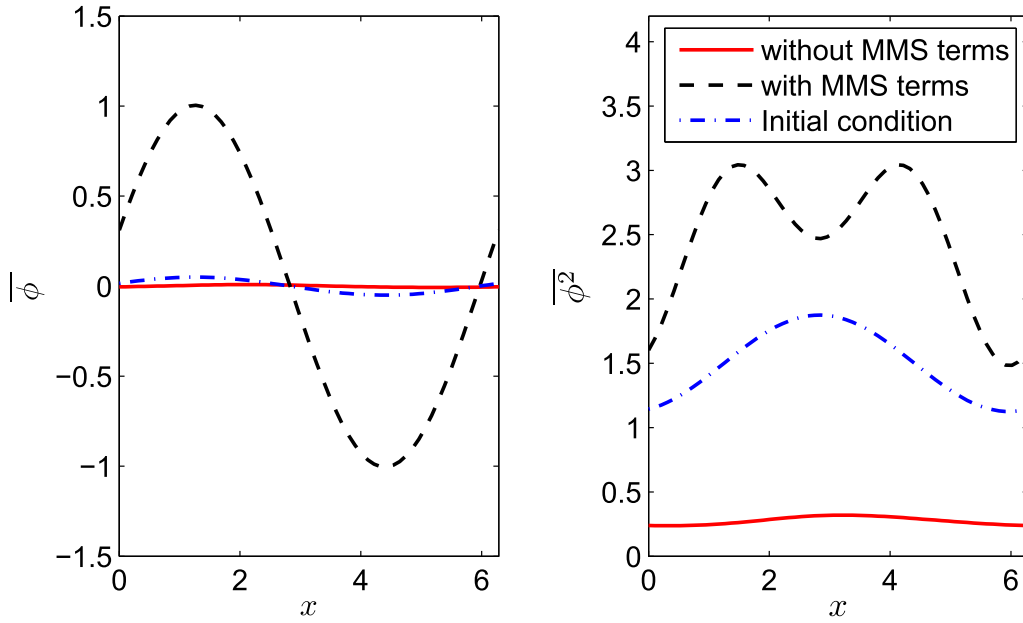
Fig. 3. The initial profiles of the first and second scalar moments and their profiles at the stopping time with and without MMS terms.
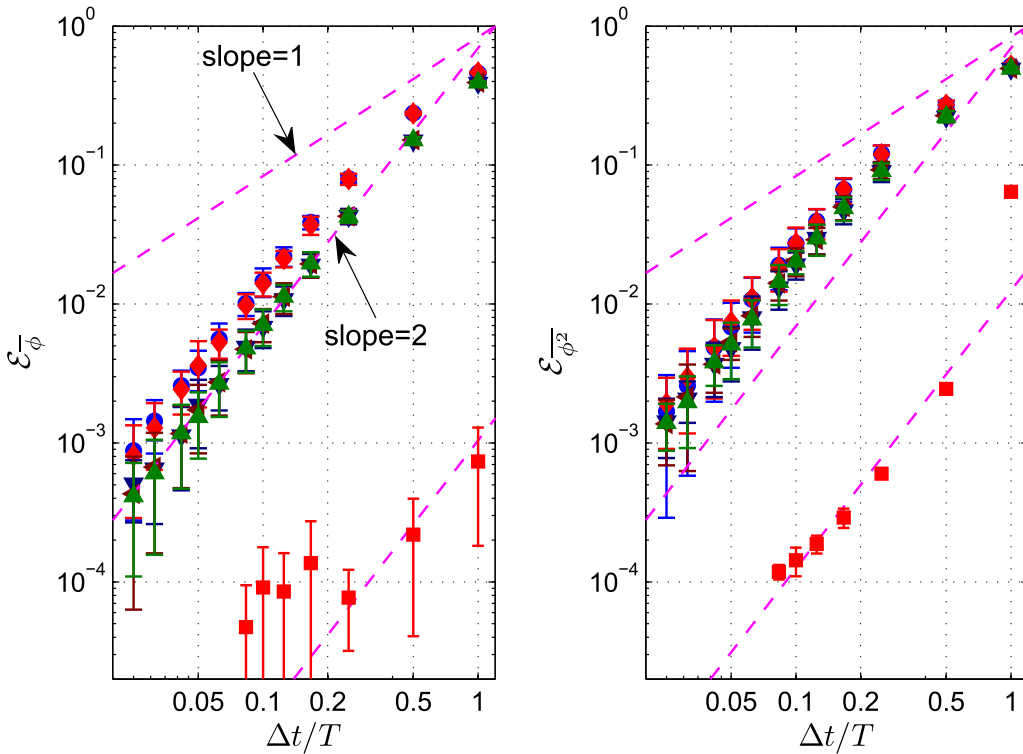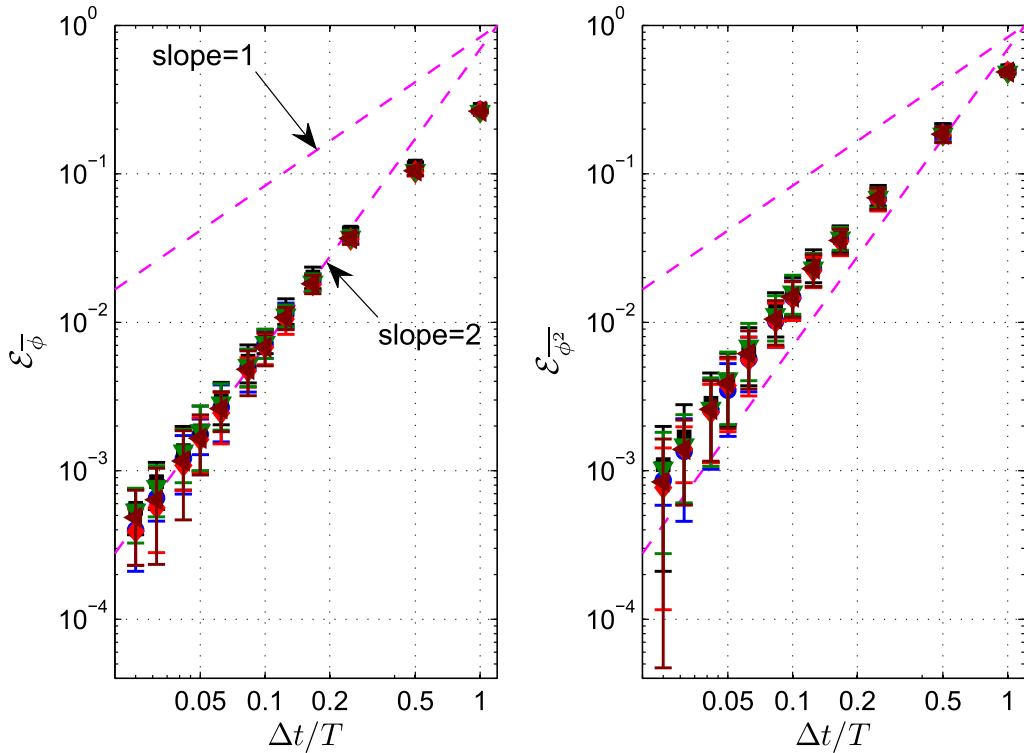

Fig. 4. The convergence of the global error of $\bar{\phi}$ and $\overline{\phi^2}$ against the time step Δt with $\mathbb{T}^{cp}\mathbb{C}\mathbb{R}\mathbb{C}'\mathbb{T}^{cp}$ in Table 3 (circle), with $\mathbb{T}^{tv}\mathbb{C}\mathbb{R}\mathbb{C}'\mathbb{T}^{tv}$ in Table 3 (diamond), with $\mathbb{T}^{cp}\mathbb{C}\mathbb{R}\mathbb{C}'\mathbb{T}^{cp}$-F in Table 4 (down triangle), with $\mathbb{T}^{tv}\mathbb{C}\mathbb{R}\mathbb{C}'\mathbb{T}^{tv}$-F in Table 4 (left triangle), with $\mathbb{T}^{kp}\mathbb{C}\mathbb{R}\mathbb{C}'\mathbb{T}^{kp}$-F in Table 4 (up triangle), and with $\mathbb{T}^{cp}\mathbb{C}\mathbb{R}\mathbb{C}'\mathbb{T}^{cp}$ in Table 3 without MMS forcing terms (square). (The error bars indicate 95% confidence intervals.)

derivative-free Ito SDE schemes, the KP scheme (3.12) and the TV scheme (3.14). One test of $\mathbb{T}^{cp}\mathbb{C}\mathbb{R}\mathbb{C}'\mathbb{T}^{cp}$ (in Table 3) without the MMS forcing terms is done and is shown as squares in Fig. 4. The test implies that the extra forcing terms introduced for the MMS do not interfere in the order of accuracy of the different splitting schemes. The numerical errors without MMS

Fig. 5. The convergence of the global error of $\bar{\phi}$ and $\overline{\phi^2}$ against the time step Δt with $\mathbb{C}\mathbb{T}^{cp}\mathbb{R}\mathbb{T}^{cp}\mathbb{C}'$ in Table 5 (circle), with $\mathbb{C}\mathbb{T}^{tv}\mathbb{R}\mathbb{T}^{tv}\mathbb{C}'$ in Table 5 (square), with $\mathbb{C}\mathbb{T}^{cp}\mathbb{R}\mathbb{T}^{cp}\mathbb{C}'$-F in Table 6 (diamond), with $\mathbb{C}\mathbb{T}^{tv}\mathbb{R}\mathbb{T}^{tv}\mathbb{C}'$-F in Table 6 (down triangle), and with $\mathbb{C}\mathbb{T}^{kp}\mathbb{R}\mathbb{T}^{kp}\mathbb{C}'$-F in Table 6 (left triangle). (The error bars indicate 95% confidence intervals.)

terms are significantly lower than those with MMS terms for the same reason given in relation to Fig. 2. The same splitting schemes on the SDE system (3.1) and (3.3) and on its frozen-coefficient counterpart (3.5) and (3.6) perform slightly differently, and the absolute error incurred by the splitting on the frozen-coefficient SDE system is a little lower than that incurred by the same splitting on the original SDE system, e.g., $\mathbb{T}^{cp}\mathbb{C}\mathbb{R}\mathbb{C}'\mathbb{T}^{cp}$ (circle) vs. $\mathbb{T}^{cp}\mathbb{C}\mathbb{R}\mathbb{C}'\mathbb{T}^{cp}$-F (down triangle) in Fig. 4. For schemes $\mathbb{T}^{cp}\mathbb{C}\mathbb{R}\mathbb{C}'\mathbb{T}^{cp}$ and $\mathbb{T}^{cp}\mathbb{C}\mathbb{R}\mathbb{C}'\mathbb{T}^{cp}$-F (and the same for schemes $\mathbb{T}^{tv}\mathbb{C}\mathbb{R}\mathbb{C}'\mathbb{T}^{tv}$ and $\mathbb{T}^{tv}\mathbb{C}\mathbb{R}\mathbb{C}'\mathbb{T}^{tv}$-F), the required time steps are in the ratio of 1:1.4 for 1% accuracy of the first scalar moment, and in the ratio of 1:1.1 for 1% accuracy of the second scalar moment approximately.

The test results of the splitting schemes of the type $\mathbb{C}\mathbb{T}\mathbb{R}\mathbb{T}\mathbb{C}'$ in Section 5.2.3 are shown in Fig. 5, $\mathbb{C}\mathbb{T}^{cp}\mathbb{R}\mathbb{T}^{cp}\mathbb{C}'$ in Table 5 (circles in Fig. 5), $\mathbb{C}\mathbb{T}^{tv}\mathbb{R}\mathbb{T}^{tv}\mathbb{C}'$ in Table 5 (squares in Fig. 5), $\mathbb{C}\mathbb{T}^{cp}\mathbb{R}\mathbb{T}^{cp}\mathbb{C}'$-F in Table 6 (diamonds in Fig. 5), $\mathbb{C}\mathbb{T}^{tv}\mathbb{R}\mathbb{T}^{tv}\mathbb{C}'$-F in Table 6 (down triangles in Fig. 5), and $\mathbb{C}\mathbb{T}^{kp}\mathbb{R}\mathbb{T}^{kp}\mathbb{C}'$-F in Table 6 (left triangles in Fig. 5). The second-order convergence of the splitting schemes is clearly indicated by the results. The difference in the performance of the different splitting schemes is not distinguishable from Fig. 5. The more detailed comparison of the different splitting schemes is discussed in the next subsection.

Fig. 6 shows the test results of the splitting schemes of type $\mathbb{C}\mathbb{R}\mathbb{T}\mathbb{C}'$ in Section 5.2.4 suitable for the current constant density test case, $\mathbb{C}\mathbb{R}\mathbb{T}^{cp}\mathbb{C}'$ in Table 7 (circles in Fig. 6), $\mathbb{C}\mathbb{R}\mathbb{T}^{tv}\mathbb{C}'$ in Table 7 (squares in Fig. 6), $\mathbb{C}\mathbb{R}\mathbb{T}^{cp}\mathbb{C}' - F$ in Table 8 (diamonds in Fig. 6), $\mathbb{C}\mathbb{R}\mathbb{T}^{tv}\mathbb{C}'$-F in Table 8 (down triangles in Fig. 6), and $\mathbb{C}\mathbb{R}\mathbb{T}^{kp}\mathbb{C}'$-F in Table 8 (left triangles in Fig. 6). The second-order accuracy of the splitting scheme is clearly shown. The frozen-coefficient SDE system is helpful to reduce the error when the same splitting scheme is used, e.g., $\mathbb{C}\mathbb{R}\mathbb{T}^{cp}\mathbb{C}'$ (circle) vs. $\mathbb{C}\mathbb{R}\mathbb{T}^{cp}\mathbb{C}'$-F (diamond), and $\mathbb{C}\mathbb{R}\mathbb{T}^{tv}\mathbb{C}'$ (square) vs. $\mathbb{C}\mathbb{R}\mathbb{T}^{tv}\mathbb{C}'$-F (down triangle) in Fig. 6. For schemes $\mathbb{C}\mathbb{R}\mathbb{T}^{cp}\mathbb{C}'$ and $\mathbb{C}\mathbb{R}\mathbb{T}^{cp}\mathbb{C}'$-F (and the same for schemes $\mathbb{C}\mathbb{R}\mathbb{T}^{tv}\mathbb{C}'$ and $\mathbb{C}\mathbb{R}\mathbb{T}^{tv}\mathbb{C}'$-F), the required time steps are in the ratio of 1:2.0 for 1% accuracy of the first scalar moment, and in the ratio of 1:1.8 for 1% accuracy of the second scalar moment approximately.

In this sub-section, we demonstrate the convergence of the different splitting schemes described in Section 5 in terms of the first and second moments. We show the convergence results of higher moments (third and fourth) for one type of splitting $\mathbb{C}\mathbb{T}\mathbb{R}\mathbb{T}\mathbb{C}'$ (Section 5.2.3) in Section 6.3. Before that, we compare the performance of different splitting schemes in the following sub-section.

6.2. Comparison of different splitting schemes

In the previous sub-section, the order of accuracy of the different splitting schemes is verified. Here, we compare the performance and efficiency of the different second-order splitting schemes.
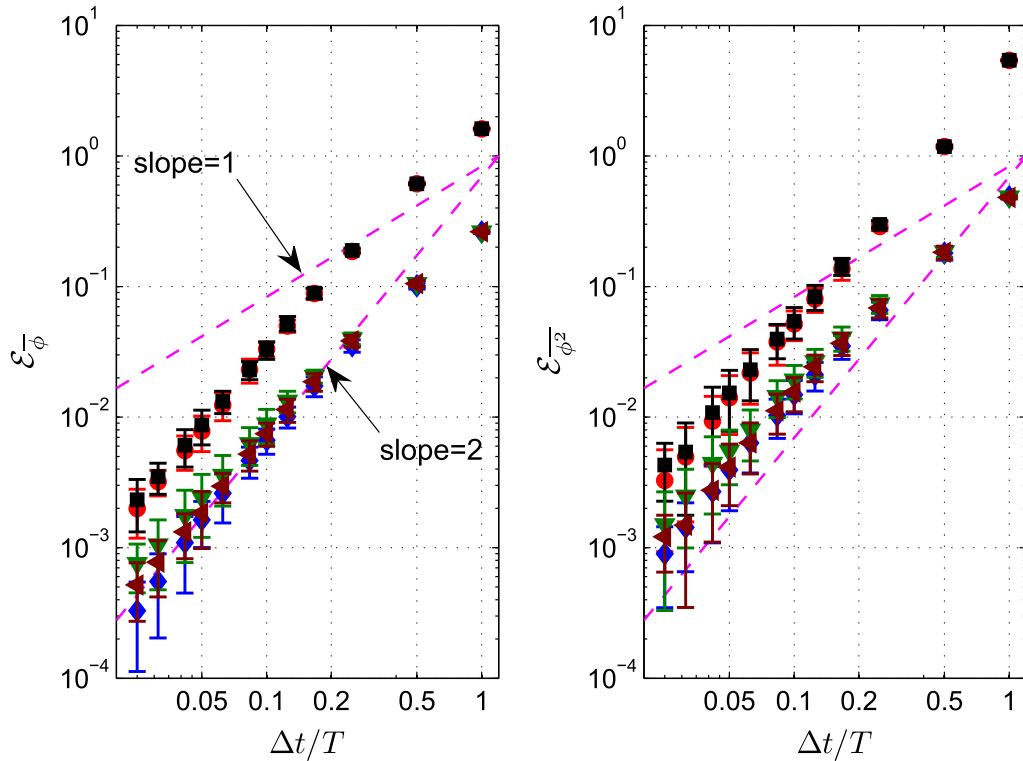
Fig. 6. The convergence of the global error of $\bar{\phi}$ and $\overline{\phi^2}$ against the time step Δt with $\mathbb{CRT^{cp}C'}$ in Table 7 (circle), with $\mathbb{CRT^{tv}C'}$ in Table 7 (square), with $\mathbb{CRT^{cp}C'}$-F in Table 8 (diamond), with $\mathbb{CRT^{tv}C'}$-F in Table 8 (down triangle), and with $\mathbb{CRT^{kp}C'}$-F in Table 8 (left triangle). (The error bars indicate 95% confidence intervals.)

The global errors of the different splitting schemes at $\Delta t = 0.05$ are compared in Table 9. Several observations can be made based on the comparison. First, the different Ito SDE schemes (CP, TV, KP) perform essentially the same when combined with the same splitting scheme according to the different columns of Table 9. The mean global errors obtained for each Ito SDE scheme are well inside of the others' 95% confidence interval. Second, comparing the same splitting schemes applied to the original SDE system (3.1) and (3.3) and to the frozen-coefficient SDE system (3.5) and (3.6), we can see that, for the most part, solving the frozen-coefficient SDE system helps to reduce the numerical error, e.g., $\mathbb{T}_1^{cp}\widehat{\mathbb{T}}_1^{cp}\mathbb{CRC'}\mathbb{T}_2^{cp}$-F incurs an error about half of that of $\mathbb{T}_1^{cp}\widehat{\mathbb{T}}_1^{cp}\mathbb{CRC'}\mathbb{T}_2^{cp}$, and the error of $\mathbb{CRTC'}$-F is about one-third of that of $\mathbb{CRTC'}$. The schemes $\mathbb{CTRTC'}$ and $\mathbb{CTRTC'}$-F are exceptions to this observation because the mean error of the scalar variance of $\mathbb{CT^{cp}RT^{cp}C'}$-F is slightly greater than that of $\mathbb{CT^{cp}RT^{cp}C'}$, and so are the mean errors of the scalar mean and variance for the TV scheme. But given the 95% confidence interval, there is no evidence that solving the frozen-coefficient SDE system incurs more error based on the existing test cases. This suggests that solving the frozen-coefficient SDE system is helpful to reduce the numerical error (or at least not to incur more numerical error than solving the original SDE system). Third, the different splitting schemes applied to the original SDE system (3.5) and (3.6) perform differently, e.g., the mean errors of $\mathbb{CRTC'}$ are about three times of those of $\mathbb{CTRTC'}$. However, when the splitting schemes are applied to the frozen-coefficient SDE system (3.5) and (3.6), the numerical errors of the different splitting schemes are indistinguishable from each other, i.e., the mean errors of one scheme are

Table 9
Comparison of the different splitting schemes combined with different Ito SDE schemes (time step $\Delta t = 0.05$) (the $\pm$ intervals indicate 95% confidence intervals).

	The CP scheme		The TV scheme		The KP scheme	
	$\mathcal{E}_{\bar{\phi}} \times 10^3$	$\mathcal{E}_{\overline{\phi^2}} \times 10^3$	$\mathcal{E}_{\bar{\phi}} \times 10^3$	$\mathcal{E}_{\overline{\phi^2}} \times 10^3$	$\mathcal{E}_{\bar{\phi}} \times 10^3$	$\mathcal{E}_{\overline{\phi^2}} \times 10^3$
$\mathbb{T}_1^{cp}\widehat{\mathbb{T}}_1^{cp}\mathbb{CRC'}\mathbb{T}_2^{cp}$	4.62 ± 1.30	7.87 ± 3.97	–	–	–	–
$\mathbb{T}_1^{cp}\widehat{\mathbb{T}}_1^{cp}\mathbb{CRC'}\mathbb{T}_2^{cp}$-F	1.59 ± 0.80	4.77 ± 1.49	–	–	–	–
$\mathbb{TCRC'T}$	3.48 ± 1.12	6.83 ± 3.36	3.60 ± 1.80	7.42 ± 3.18	–	–
$\mathbb{TCRC'T}$-F	1.88 ± 0.97	4.80 ± 2.03	1.73 ± 0.89	5.31 ± 1.35	1.54 ± 0.77	5.11 ± 2.24
$\mathbb{CTRTC'}$	1.76 ± 0.47	3.48 ± 1.78	1.86 ± 0.86	4.10 ± 2.09	–	–
$\mathbb{CTRTC'}$-F	1.62 ± 0.66	3.75 ± 1.92	1.87 ± 0.87	4.18 ± 2.13	1.66 ± 0.72	3.88 ± 1.95
$\mathbb{CRTC'}$	7.82 ± 2.38	14.08 ± 6.72	8.71 ± 2.58	15.31 ± 7.52	–	–
$\mathbb{CRTC'}$-F	1.63 ± 0.63	3.94 ± 2.02	2.42 ± 1.22	5.50 ± 2.47	1.84 ± 0.86	4.15 ± 2.05

inside of others' 95% confidence intervals. This suggests that the difference in performance of the different splitting schemes on the original SDE system can be reduced by using them instead on the frozen-coefficient SDE system.

The computational cost of the different splitting schemes are compared in Table 10 in terms of micro-seconds (μs) per particle per time step. First, the computational cost of the different splitting schemes is slightly different, e.g., for the CP scheme, the least expensive scheme $\mathbb{CRTC}'$ is about 20% quicker than the most expensive scheme $\mathbb{TCRC}'\mathbb{T}$, and for the same splitting $\mathbb{TCRC}'\mathbb{T}$-F, the least expensive scheme TV is about 10% quicker than the most expensive scheme KP. Second, the overall computational cost of about $3\mu s$ per particle per time step of the test case is cheap. (The computational cost of the three-dimensional case is certainly higher but will not increase in order of magnitude. And also the above cost includes the evaluation of the manufactured solutions in Appendix C which is estimated to be over 60% of the overall cost and is not needed in the real PDF simulations.) It is estimated that the computational cost of a PDF code featuring detailed chemistry using ISAT is about 10 to 100 μs per particle per time step. So the cost of the particle transport and mixing (with simple mixing models) is only a very small portion of the total cost, and choosing different Ito SDE schemes and the different splitting schemes does not change the total computational cost of the PDF applications significantly.

6.3. Convergence of high moments

The weak convergence of the SDE schemes and splitting schemes has been verified for the first and second moments in Section 6.1. For completeness, we also perform the convergence tests for the second-order splitting schemes discussed in this paper in terms of the third and fourth moments. The tests confirm the second-order convergence of all the second-order splitting schemes discussed in Section 5. For brevity, here we present the convergence results for only one type of splitting $\mathbb{CTRTC}'$ in Section 5.2.3. The analytical solutions of the third and fourth moments are not known for the estimate of numerical error in the test. We perform a high resolution finite-difference simulation of the transport equations of the third and fourth moments to obtain an accurate estimate of their exact solutions. The transport equations for the third and fourth scalar moments derived from the PDF transport Eq. (4.4) are

$$\frac{\partial \overline{\phi^3}(\mathbf{x},t)}{\partial t} + \frac{\partial \bar{u}_i(\mathbf{x},t)\overline{\phi^3}(\mathbf{x},t)}{\partial x_i} = \frac{\partial}{\partial x_i}\left(\Gamma(\mathbf{x},t)\frac{\partial \overline{\phi^3}(\mathbf{x},t)}{\partial x_i}\right) - 3\Omega(\mathbf{x},t)\left(\overline{\phi^3}(\mathbf{x},t) - \overline{\phi^2}_m(\mathbf{x},t)\bar{\phi}_m(\mathbf{x},t)\right)$$
$$+ 3R_a\left(\overline{\phi^3}(\mathbf{x},t) - R_b\overline{\phi^2}_m(\mathbf{x},t)\right) + 3S_m(\mathbf{x},t)\overline{\phi^2}_m(\mathbf{x},t)$$
$$- 3\Omega_v(\mathbf{x},t)\left(\overline{\phi^3}(\mathbf{x},t) - \overline{\phi^2}_m(\mathbf{x},t)\bar{\phi}_m(\mathbf{x},t)\right), \tag{6.2}$$

$$\frac{\partial \overline{\phi^4}(\mathbf{x},t)}{\partial t} + \frac{\partial \bar{u}_i(\mathbf{x},t)\overline{\phi^4}(\mathbf{x},t)}{\partial x_i} = \frac{\partial}{\partial x_i}\left(\Gamma(\mathbf{x},t)\frac{\partial \overline{\phi^4}(\mathbf{x},t)}{\partial x_i}\right) - 4\Omega(\mathbf{x},t)(\overline{\phi^4}(\mathbf{x},t) - \overline{\phi^3}(\mathbf{x},t)\bar{\phi}_m(\mathbf{x},t)) + 4R_a(\overline{\phi^4}(\mathbf{x},t)$$
$$- R_b\overline{\phi^3}(\mathbf{x},t)) + 4S_m(\mathbf{x},t)\overline{\phi^3}(\mathbf{x},t) - 4\Omega_v(\mathbf{x},t)(\overline{\phi^4}(\mathbf{x},t) - \overline{\phi^3}(\mathbf{x},t)\bar{\phi}_m(\mathbf{x},t)). \tag{6.3}$$

The equations are in closed form and can be solved numerically. Given the initial Gaussian distribution which is used in the particle initialization and the manufactured solutions for the first and second moments, we obtain the initial conditions for the numerical solutions of Eqs. (6.2) and (6.3) as follows:

$$\overline{\phi^3}(\mathbf{x},0) = 3\bar{\phi}_m(\mathbf{x},0)\overline{\phi^2}_m(\mathbf{x},0) - 2\bar{\phi}_m^3(\mathbf{x},0), \tag{6.4}$$
$$\overline{\phi^4}(\mathbf{x},0) = 3\overline{\phi^2}_m^2(\mathbf{x},0) - 2\bar{\phi}_m^4(\mathbf{x},0), \tag{6.5}$$

where $\bar{\phi}_m$ and $\overline{\phi^2}_m$ are from Eqs. (C.1) and (C.3).

We obtain an accurate numerical solution of Eqs. (6.2) and (6.3) using a finite-difference method. The equations are discretized by central-differences in space and Crank–Nicolson scheme in time, yielding second-order accuracy in space and time. A total of 7500 grid cells are used in the simulation, and the time step is controlled to have the CFL number less than one, resulting in about 6000 time steps in total. The obtained numerical solutions from Eqs. (6.2) and (6.3) are used for

Table 10
Computational cost of the different splitting schemes in terms of μs per particle per time step.

	The CP scheme	The TV scheme	The KP scheme
$\mathbb{T}_1^{cp}\hat{\mathbb{T}}_1^{cp}\mathbb{CRC}'\mathbb{T}_2^{cp}$	2.63	–	–
$\mathbb{T}_1^{cp}\hat{\mathbb{T}}_1^{cp}\mathbb{CRC}'\mathbb{T}_2^{cp}$-F	2.66	–	–
$\mathbb{TCRC}'\mathbb{T}$	3.23	3.01	–
$\mathbb{TCRC}'\mathbb{T}$-F	3.22	3.03	3.34
$\mathbb{CTRTC}'$	3.18	3.02	–
$\mathbb{CTRTC}'$-F	3.20	3.07	3.33
$\mathbb{CRTC}'$	2.46	2.39	–
$\mathbb{CRTC}'$-F	2.49	2.38	2.54
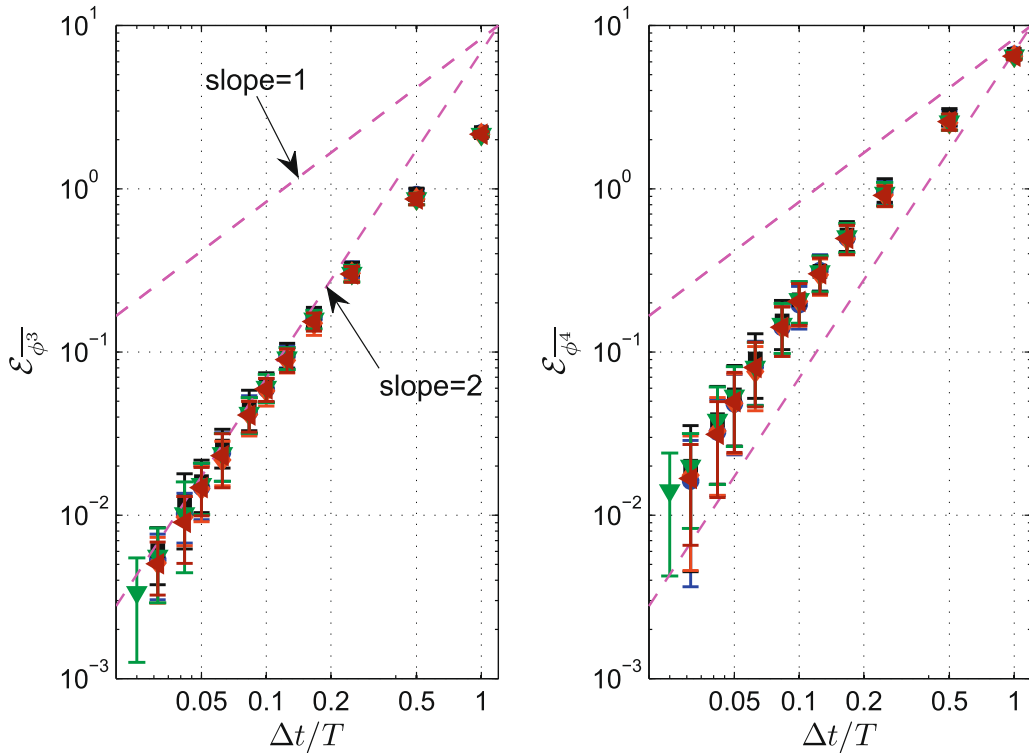
Fig. 7. The convergence of the global error of $\overline{\phi^3}$ and $\overline{\phi^4}$ against the time step Δt with $\mathbb{CT}^{cp}\mathbb{RT}^{cp}\mathbb{C}'$ in Table 5 (circle), with $\mathbb{CT}^{tv}\mathbb{RT}^{tv}\mathbb{C}'$ in Table 5 (square), with $\mathbb{CT}^{cp}\mathbb{RT}^{cp}\mathbb{C}'$-F in Table 6 (diamond), with $\mathbb{CT}^{tv}\mathbb{RT}^{tv}\mathbb{C}'$-F in Table 6 (down triangle), and with $\mathbb{CT}^{kp}\mathbb{RT}^{kp}\mathbb{C}'$-F in Table 8 (left triangle). (The error bars indicate 95% confidence intervals.)

estimating global errors (4.10) of the third and fourth moments sampled from the particles. The results of the convergence test for schemes $\mathbb{CTRTC}'$ (Section 5.2.3) are shown in Fig. 7. The test cases in the figure are the same as those in Fig. 5. From the figure, clearly we can see that the splitting schemes are second-order convergent for the third and fourth moments. The convergence tests are performed for all the second-order splitting schemes discussed in Section 5, and the test results confirm the second-order convergence. (These test results are not shown.)

7. Discussion

In the convergence tests performed in Section 6, the simplifications of one dimension, single scalar and constant density have been made. The developed splitting schemes in Section 5.2.1,5.2.2,5.2.3 can be applied to all general three-dimensional, multi-scalar and variable-density problems. (The three-dimensional versions of the TV scheme and KP scheme in Section 3.3 must be used which can be found in the respective references. Any other weak second-order Ito SDE schemes can be used for the splitting. And the scalar equations are not limited to contain only the processes discussed.) The splitting scheme of the type $\mathbb{CRTC}'$ in Section 5.2.4 is designed for the non-coupled case between the reaction and the transport, e.g., constant density. It features only one step of reaction and one step of transport in the splitting. This splitting can also be used in the variable-density case without the feedback of density from the particle system to the flow solver, i.e., the reaction and the transport are independent, and the flow solver has its own estimate of density. This no-feedback configuration is a good study case for the development of PDF algorithms and code. It is also possible to apply the splitting $\mathbb{CRTC}'$ to the coupled variable-density problems. For example, if a second-order time extrapolation of the density is already obtained to perform the second sub-step of transport in $\mathbb{CTRTC}'$, then this splitting might be possibly reduced to $\mathbb{CRTC}'$ still with second-order accuracy. The formal order of accuracy of $\mathbb{CRTC}'$ in variable-density problems certainly needs further investigation in the future.

In the development of the MMS for the particle method, the linear reaction (4.1) is specified which is required for the closure of the moment Eqs. (2.3) and (2.4) for weak convergence. This specification is introduced for verification purposes only. Any complex (non-linear) reaction mechanism can be incorporated in the PDF methods without approximation. And the weak second-order accuracy of the splitting holds for the non-linear system. Due to sub-stepping, the reaction sub-step (5.2) is separated from the system and is independent from the particle position $\mathbf{X}(t)$. As far as the reaction sub-step is integrated stably with at least second-order accuracy, the splitting schemes (with second-order accuracy for the linear system)

developed in this paper are still second-order accurate. The developed MMS for Monte Carlo particle methods can be applied to general problems with multi-dimension, multi-scalar and variable-density. In the design of the manufactured solutions, although the original PDF transport Eq. (2.1) is not satisfied by the manufactured solutions in general, the continuity equation is often chosen to be satisfied by the manufactured solutions due to the significance of mass conservation in our problem [44]. (Manufactured solutions without mass conservation are certainly possible for verification purposes, in which case a mass changing process is introduced.)

The convergence of the different splitting schemes discussed in this work is verified based on a one-dimensional test case. This test case is representative as far as non-trivial variations in the manufactured solutions are specified and proper initial and boundary conditions are imposed. In Appendix C, the manufactured solutions to the test case are specified which have non-trivial variations. Notice that the velocity component $\bar{u}$ (C.4) is uniform to satisfy the continuity equation. However, in the Ito SDE (2.6), the velocity always appears in the form of the drift velocity $D = \bar{u} + \nabla\Gamma$. As far as the diffusivity Γ (C.5) has a non-trivial gradient, the drift velocity D has non-trivial variation in space. The test case is periodic in space, so the periodic boundary condition is imposed on particles' positions. The test can be straightforwardly extended to three-dimensional general test cases with other types of boundary conditions. The only concern with the extension is the computational cost which might be prohibitive when the test case is more complicated. Simple functions (e.g., a single sine or cosine mode with long wave length and time period) are suggested to design the manufactured solutions in order to take a relatively longer time step and larger grid size but still having the desired asymptotic convergent behavior.

In this work, only the time convergence of the Monte Carlo particle method is considered. In the Monte Carlo particle method it is not necessary to have a grid. However, in practice, the SDE coefficients are usually obtained from grid-based methods and are stored on a grid. The interpolation of these grid level SDE coefficients to the particles involves spatial error. The estimate of the particle scalar mean (5.6) for the IEM model often requires a grid to have sufficient particles inside a grid level, which involves a spatial smearing error. Hence the grid convergence of the Monte Carlo particle method also needs to be addressed. Some discussion has been made in a previous work [50]. The developed MMS for the particle method is applicable to the verification of the grid convergence of the particle method. Notice that, if a second-order spatial accurate method is used, in order to verify the grid convergence the computational cost scales as Δx^{-5}, where Δx is the grid size and Δt is fixed for different Δx in the estimate. Hence a simple test case is suggested to make the computational cost affordable.

The TV Ito SDE scheme (3.14) involves the specification of two free parameters α_2 and μ_3 and the choice between two families of parameters, (3.16) or (3.17). In all the results presented in Section 6, constants $\alpha_2 = 1.0$ and $\mu_3 = 0.5$ and parameters (3.17) are used. In addition, a set of tests is performed with $\alpha_2 \in [0.5, 10]$ and $\mu_3 \in [-100, 10]$ for (3.17) and with $\alpha_2 = 1.0$ and $\mu_3 = 0.5$ for (3.16). No significant difference is found among all these tests in terms of accuracy and efficiency of the scheme. All choices of the constants result in the same number of coefficient evaluations for the one-dimensional version of the scheme, i.e., no simplification of the scheme. In the KP scheme (3.12), the random variable ξ can be specified as a three-point distributed random number (3.13) rather than a standardized Gaussian random number. The weak second-order accuracy of the scheme with this three-point distributed random number is confirmed by the test. No significant difference in the accuracy and efficiency is found when compared to the standardized Gaussian random number.

Among the splitting schemes discussed in this work, the splitting schemes for the frozen-coefficient SDE system are usually a little more accurate than those for the original SDE system. Other than that, no significant difference in accuracy and efficiency is found among the different splitting schemes. In RANS/PDF or LES/FDF applications, there might be additional considerations for choosing one scheme over others. The splitting schemes for the frozen-coefficient SDE system require only
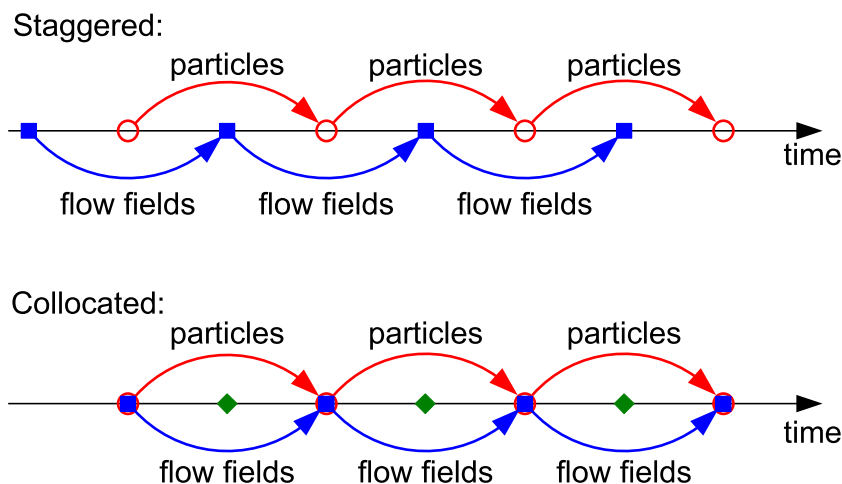
Fig. 8. Staggered and collocated arrangement of flow fields and particles in time. (The circles are the time levels of particles, and the solid squares are the time levels to store flow fields (velocity and diffusivity etc.). The solid lines with arrows indicate the time advancement step for particles and flow fields. The solid diamonds indicate the flow fields at the mid-time interpolated from the neighbors.)

one time level of flow fields (at the mid-time in the particle step) for particle advancement, while those for the original SDE system require at least two time levels of flow fields, e.g., $\mathbb{T}_1^{cp}\widehat{\mathbb{T}}_1^{cp}\mathbb{C}\mathbb{R}\mathbb{C}'\mathbb{T}_2^{cp}$ in Table 2 requires two levels of flow fields (at t_0 and $t_{\frac{1}{2}}$) and $\mathbb{T}^{cp}\mathbb{C}\mathbb{R}\mathbb{C}'\mathbb{T}^{cp}$ in Table 3 requires four levels of flow fields (at $t_0, t_{\frac{1}{4}}, t_{\frac{1}{2}},$ and $t_{\frac{3}{4}}$). To implement the splitting schemes for the original SDE system, at least two time levels of flow fields are needed in the particle solver to interpolate or extrapolate the required flow fields. The use of the frozen-coefficient splitting schemes simplifies the coupling between the flow solver and the particle solver, and reduces the storage requirement of the particle code because only one time level of flow fields is needed in the particle solver. Another coupling issue between the flow solver and the particle solver is the time arrangement of the flow fields in the flow solver and the particles in the particle solver. There are usually two kinds of time arrangements of the flow fields and particles: staggered and collocated, as shown in Fig. 8. The splitting schemes for the frozen-coefficient SDE are applicable to both of them. In the staggered arrangement, the flow fields are stored at the mid-time of the particle step, so the flow fields are used naturally for the particle time advancement. In the collocated arrangement, the flow fields and particles are stored at the same time level, so the required mid-time flow fields for the particle time advancement need to be interpolated or extrapolated from the adjacent flow fields. There are some other issues in the coupling between the flow solver and particle solver, e.g., in a fully coupled variable-density LES/FDF code, iteration of the flow time step and particle time step may be needed. This is beyond the discussion of this work and will be addressed in the future work.

8. Conclusions

In this work, different weak second-order splitting schemes for solving the SDE system from the composition PDF methods are developed. Three Ito SDE schemes from the literature are chosen for investigation, the CP scheme (3.10), the KP scheme (3.12) and the TV scheme (3.14). A frozen-coefficient SDE system (3.5) and (3.6) is proposed as an alternative system to solve. The MMS for the Monte Carlo particle method is developed, in which the augmented scalar moment equations and the augmented particle scalar equation are derived. Different types of splitting schemes (on the original SDE system or on the frozen-coefficient SDE system) are discussed. The formal order of accuracy of the different splitting schemes is demonstrated by the particle MMS with a one-dimensional test case. The first-order accuracy of the CP scheme simply coupled with the scalar equation is shown, and it is shown that second-order accuracy is achieved by introducing a modified mid-point. The second-order accuracy of the other proposed splitting schemes is verified. The different second-order splitting schemes are compared in terms of accuracy and efficiency. The comparison suggests that solving the original SDE system with different splitting schemes yields somewhat different numerical errors, and that solving the frozen-coefficient SDE system helps to reduce the numerical error, and to reduce the difference of the numerical errors yielded by the different splitting schemes. No other significant difference is found in the comparison in terms of accuracy and efficiency of the different splitting schemes. This is a useful conclusion in that there is a considerable range of accurate and efficient schemes that can be implemented; and in practice there may be additional considerations and constraints which favor one scheme over others. The applicability and extensibility of the developed methodologies to the general three-dimensional, multi-scalar and variable-density problems are briefly discussed.

Acknowledgments

Appendix A. Proof of the SDE system with frozen coefficients

We prove that the solutions of the SDEs with frozen coefficients (3.5) and (3.6) are consistent with those of the original SDEs (3.1) and (3.3) to order Δt^2 for one time step in the weak sense (i.e., the difference between the solutions is of order Δt^3). For weak second-order numerical schemes, the numerical solutions are consistent with the exact solutions to Δt^2 for one time step in the weak sense. Hence this proof guarantees the equivalence of solving (3.1) and (3.3), and (3.5) and (3.6) with second-order accuracy.

A.1. Proof of the frozen-coefficient Ito SDE[2]

We first prove that the solution of (3.5) is consistent with that of (3.1) to order Δt^2 for one time step in the weak sense. According to the sufficient conditions for weak second-order accuracy obtained in [25], we only need to verify the consistency of the first four moments of ΔX from (3.1) and (3.5).

Following [25], we consider one integration step $[0, \Delta t]$ (i.e., $t_0 = 0$), from the deterministic initial condition $\mathbf{X}(0) = \mathbf{X}'(0) = 0$, then $\Delta \mathbf{X} = \mathbf{X}(\Delta t)$ and $\Delta \mathbf{X}' = \mathbf{X}'(\Delta t)$, where $\mathbf{X}$ and $\mathbf{X}'$ denote the numerical solutions to (3.1) and (3.5), respectively. The moments of $\mathbf{X}$ can be obtained from its PDF $f(\mathbf{x}; t)$ and the Fokker–Planck equation. The first four moments of $\Delta \mathbf{X}$ for (3.1) are [25]

---

[2] Using the corresponding Fokker–Planck equation seems a natural starting point for the proof, but we are not successful in that direction.

$$E(\Delta X_p) = \Delta t D_p^0 + \Delta t^2 \left(\frac{1}{2} D_j^0 D_{p,j}^0 + \frac{1}{4} b^0 D_{p,jj}^0 + \frac{1}{2} \dot{D}_p^0 \right) + O(\Delta t^3), \tag{A.1}$$

$$E(\Delta X_p \Delta X_q) = \Delta t b^0 \delta_{pq} + \Delta t^2 \left(D_p^0 D_q^0 + \frac{1}{2} b^0 \left(D_{p,q}^0 + D_{q,p}^0 \right) + \frac{1}{2} \delta_{pq} D_j^0 b_j^0 + \frac{1}{4} b^0 b_{jj}^0 \delta_{pq} + \frac{1}{2} \dot{b}^0 \delta_{pq} \right) + O(\Delta t^3), \tag{A.2}$$

$$E(\Delta X_p \Delta X_q \Delta X_r) = \Delta t^2 \left(b^0 \left(D_p^0 \delta_{qr} + D_q^0 \delta_{pr} + D_r^0 \delta_{pq} \right) + \frac{1}{2} b^0 \left(b_{,p}^0 \delta_{qr} + b_{,q}^0 \delta_{pr} + b_{,r}^0 \delta_{pq} \right) \right) + O(\Delta t^3), \tag{A.3}$$

$$E(\Delta X_p \Delta X_q \Delta X_r \Delta X_s) = \Delta t^2 (b^0)^2 (\delta_{pq} \delta_{rs} + \delta_{pr} \delta_{qs} + \delta_{ps} \delta_{qs}) + O(\Delta t^3), \tag{A.4}$$

where the superscript "0" denotes the evaluation at the initial position ($\mathbf{X}(0) = 0$) and initial time ($t = 0$), and other quantities appearing in these equations are defined as $D_{i,j} \equiv \partial D_i / \partial X_j, D_{i,jj} \equiv \partial^2 D_i / \partial X_j \partial X_j, \dot{D}_i \equiv \partial D_i / \partial t, b_{,j} \equiv \partial b / \partial X_j, b_{,jj} \equiv \partial^2 b / \partial X_j X_j$, and $\dot{b} \equiv \partial b / \partial t$.

The frozen-coefficient Ito SDE (3.5) is a special case of the SDE (3.1), i.e., eliminating the dependence of the coefficients D_i and b on time and freezing the coefficients at the mid-time $\left(t = t_{\frac{1}{2}} = \frac{1}{2} \Delta t \right)$. From (A.1) to (A.4), we can readily obtain the first four moments of $\Delta \mathbf{X}'$ for (3.5)

$$E\left(\Delta X_p' \right) = \Delta t D_p^* + \Delta t^2 \left(\frac{1}{2} D_j^* D_{p,j}^* + \frac{1}{4} b^* D_{p,jj}^* \right) + O(\Delta t^3), \tag{A.5}$$

$$E\left(\Delta X_p' \Delta X_q' \right) = \Delta t b^* \delta_{pq} + \Delta t^2 \left(D_p^* D_q^* + \frac{1}{2} b^* \left(D_{p,q}^* + D_{q,p}^* \right) + \frac{1}{2} \delta_{pq} D_j^* b_j^* + \frac{1}{4} b^* b_{jj}^* \delta_{pq} \right) + O(\Delta t^3), \tag{A.6}$$

$$E\left(\Delta X_p' \Delta X_q' \Delta X_r' \right) = \Delta t^2 \left(b^* \left(D_p^* \delta_{qr} + D_q^* \delta_{pr} + D_r^* \delta_{pq} \right) + \frac{1}{2} b^* \left(b_{,p}^* \delta_{qr} + b_{,q}^* \delta_{pr} + b_{,r}^* \delta_{pq} \right) \right) + O(\Delta t^3), \tag{A.7}$$

$$E\left(\Delta X_p' \Delta X_q' \Delta X_r' \Delta X_s' \right) = \Delta t^2 (b^*)^2 (\delta_{pq} \delta_{rs} + \delta_{pr} \delta_{qs} + \delta_{ps} \delta_{qs}) + O(\Delta t^3), \tag{A.8}$$

where the superscript "*" denotes the evaluation at the initial position ($\mathbf{X}'(0) = 0$) and mid-time $\left(t = t_{\frac{1}{2}} \right)$.

Expanding the coefficient (D_i^*, b^* and their spatial derivatives) at $t = 0$, we obtain

$$G^* = G^0 + \dot{G}^0 \frac{\Delta t}{2} + O(\Delta t^2), \tag{A.9}$$

where G is any one of the coefficients and their derivatives in (A.5)–(A.8).

Substituting the Taylor series expansions (A.9) into (A.5)–(A.8) and collecting all the leading order terms, we have

$$E\left(\Delta X_p' \right) = \Delta t D_p^0 + \Delta t^2 \left(\frac{1}{2} D_j^0 D_{p,j}^0 + \frac{1}{4} b^0 D_{p,jj}^0 + \frac{1}{2} \dot{D}_p^0 \right) + O(\Delta t^3), \tag{A.10}$$

$$E\left(\Delta X_p' \Delta X_q' \right) = \Delta t b^0 \delta_{pq} + \Delta t^2 \left(D_p^0 D_q^0 + \frac{1}{2} b^0 \left(D_{p,q}^0 + D_{q,p}^0 \right) + \frac{1}{2} \delta_{pq} D_j^0 b_j^0 + \frac{1}{4} b^0 b_{jj}^0 \delta_{pq} + \frac{1}{2} \dot{b}^0 \delta_{pq} \right) + O(\Delta t^3), \tag{A.11}$$

$$E\left(\Delta X_p' \Delta X_q' \Delta X_r' \right) = \Delta t^2 \left(b^0 \left(D_p^0 \delta_{qr} + D_q^0 \delta_{pr} + D_r^0 \delta_{pq} \right) + \frac{1}{2} b^0 \left(b_{,p}^0 \delta_{qr} + b_{,q}^0 \delta_{pr} + b_{,r}^0 \delta_{pq} \right) \right) + O(\Delta t^3), \tag{A.12}$$

$$E(\Delta X_p' \Delta X_q' \Delta X_r' \Delta X_s') = \Delta t^2 (b^0)^2 (\delta_{pq} \delta_{rs} + \delta_{pr} \delta_{qs} + \delta_{ps} \delta_{qs}) + O(\Delta t^3). \tag{A.13}$$

Evidently, with the same initial condition $\mathbf{X}(0) = \mathbf{X}'(0)$, (A.10)–(A.13) are consistent with (A.1)–(A.4) to order Δt^2. Thus the SDEs (3.1) and (3.5) are equivalent when solved with weak second-order SDE schemes.

A.2. Proof of the frozen-coefficient scalar equation

We now prove the equivalence of solving scalar Eqs. (3.3) and (3.6) to second-order accuracy. For simplicity, we consider one step integration $[0, \Delta t]$ with the same Ito process $\mathbf{X}(t)$ in (3.3) and (3.6) and with the initial condition $\phi(0) = \phi'(0) = \phi_0$.

Eq. (3.3) is

$$\frac{d\phi(t)}{dt} = A(\mathbf{X}(t), \phi(t), t) = A\left(\mathbf{X}(t), \phi_0 + \Delta\phi(t), t_{\frac{1}{2}} + \left(t - t_{\frac{1}{2}} \right) \right) = A + A_\phi \Delta\phi(t) + \dot{A}\left(t - t_{\frac{1}{2}} \right) + O(\Delta t^2), \tag{A.14}$$

for $t = O(\Delta t), A_\phi$ and $\dot{A}$ denote derivatives of A with respect to the second and third arguments, and in the last line A, A_ϕ and $\dot{A}$ are evaluated at $\left(\mathbf{X}(t), \phi_0, t_{\frac{1}{2}} \right)$.

Similarly, (3.6) is

$$\frac{d\phi'(t)}{dt} = A + A_\phi \Delta\phi'(t) + O(\Delta t^2), \tag{A.15}$$

where A and A_ϕ, being evaluated at $\left(\mathbf{X}(t), \phi_0, t_{\frac{1}{2}} \right)$, are identical in the above two equations. Thus, the difference $\phi - \phi'$ evolve by

$$\frac{d(\phi(t) - \phi'(t))}{dt} = A_\phi(\phi(t) - \phi'(t)) + \dot{A}\left(t - t_{\frac{1}{2}} \right) + O(\Delta t^2). \tag{A.16}$$

Since $\phi'(t)$ is certainly at least a first-order approximation to $\phi(t)$, it follows that the difference $\phi(t) - \phi'(t)$ is of order Δt^2 (or higher), and the first term on the right-hand side of (A.16) when integrated over $[0, \Delta t]$ is of order Δt^3 (or higher). It is readily shown that the second term on the right-hand side of (A.16) when integrated over $[0, \Delta t]$ is also of order Δt^3. Thus the difference $\phi(t) - \phi'(t)$ is of order Δt^3, confirming the second-order accuracy of (3.6) with frozen coefficients.

Appendix B. Measurement of the global error for weak convergence

The error $e_{q,i,k}$ (4.8) estimates the local deterministic error $\mu_{q,i}$ from the kth trial. If the number of particles used in the trial is small, this estimate involves large statistical error. Here, we derive an un-biased estimate of the global error $\mathcal{E}_{\overline{\phi^q}}$ (4.10) based on $e_{q,i,k}$ from all the grids and all the trials performed to reduce the effect of the statistical error.

From (4.9), we can obtain

$$e_{q,i,k}^2 = \mu_{q,i}^2 + \sigma_{q,i}^2 \xi_{q,i,k}^2 + 2\mu_{q,i}\sigma_{q,i}\xi_{q,i,k}. \tag{B.1}$$

We take the average of (4.9) and (B.1) over K independent trials

$$\langle e_{q,i}\rangle^* = \mu_{q,i} + \sigma_{q,i}\frac{1}{K}\sum_{k=1}^{K}\xi_{q,i,k}, \tag{B.2}$$

$$\langle e_{q,i}^2\rangle^* = \mu_{q,i}^2 + \sigma_{q,i}^2\frac{1}{K}\sum_{k=1}^{K}\xi_{q,i,k}^2 + 2\mu_{q,i}\sigma_{q,i}\frac{1}{K}\sum_{k=1}^{K}\xi_{q,i,k}. \tag{B.3}$$

From (B.2), we obtain

$$\langle e_{q,i}\rangle^{*2} = \mu_{q,i}^2 + \sigma_{q,i}^2\frac{1}{K^2}\sum_{k=1}^{K}\xi_{q,i,k}^2 + 2\mu_{q,i}\cdot\sigma_{q,i}\frac{1}{K}\sum_{k=1}^{K}\xi_{q,i,k} + \sigma_{q,i}^2\frac{1}{K^2}\sum_{k=1}^{K}\sum_{l=1,l\neq k}^{K}\xi_{q,i,k}\xi_{q,i,l}. \tag{B.4}$$

The expectation of (B.3) and (B.4) are

$$E\left(\left\langle e_{q,i}^2\right\rangle^*\right) = \mu_{q,i}^2 + \sigma_{q,i}^2, \tag{B.5}$$

$$E(\langle e_{q,i}\rangle^{*2}) = \mu_{q,i}^2 + \frac{\sigma_{q,i}^2}{K}. \tag{B.6}$$

Solving (B.5) and (B.6) for $\mu_{q,i}$, we obtain

$$\mu_{q,i}^2 = \frac{1}{1-1/K}\left(E(\langle e_{q,i}(\overline{\phi^q})\rangle^{*2}) - \frac{1}{K}E\left(\left\langle e_{q,i}^2(\overline{\phi^q})\right\rangle^*\right)\right). \tag{B.7}$$

Based on (B.7), we can construct an un-biased estimate of $\mu_{q,i}^2$ from the numerical simulation

$$\mu_{q,i}^2 \approx \frac{1}{1-1/K}\left(\langle e_{q,i}\rangle^{*2} - \frac{1}{K}\left\langle e_{q,i}^2\right\rangle^*\right). \tag{B.8}$$

The value of $\mu_{q,i}^2$ is a local measure of the time-stepping error ($\mu_{q,i} \propto \Delta t^p$ for pth order convergence). A global measure of the time-stepping error is defined in (4.10). Apparently, $E(\mathcal{E}_{\overline{\phi^q}}) \propto \Delta t^p$ for pth order convergence too.

Substituting (B.8) into (4.10), we obtain the un-biased estimate of the global error

$$\mathcal{E}_{\overline{\phi^q}} = \left[\frac{1}{I}\sum_{i=1}^{I}\frac{1}{1-1/K}\left(\langle e_{q,i}\rangle^{*2} - \frac{1}{K}\left\langle e_{q,i}^2\right\rangle^*\right)\right]^{1/2}. \tag{B.9}$$

Note that, in practice, a valid value of $\mathcal{E}_{\overline{\phi^q}}$ may not be obtained because the summation under the square-root in (B.9) may be negative. If this happens, more particles or trials are required.

Appendix C. Manufactured solutions to one-dimensional test case

For the one-dimensional, periodic, constant-density problem $x \in [0, L_0]$ and $t \in [0, T]$, the manufactured analytical solutions to (4.2) and (4.3) are specified as:

$$\bar{\phi}_m(x,t) = \frac{1}{20}e^{3\varpi t}\cos\left(2\pi\kappa x - \frac{12}{5}\pi\right), \tag{C.1}$$

$$\overline{\phi'^2}_m(x,t) = \frac{1}{8}\left(4 - e^{-3\varpi t}\right)\left[\sin\left(2\pi\kappa x - \frac{12}{5}\pi\right) + 4\right]. \tag{C.2}$$

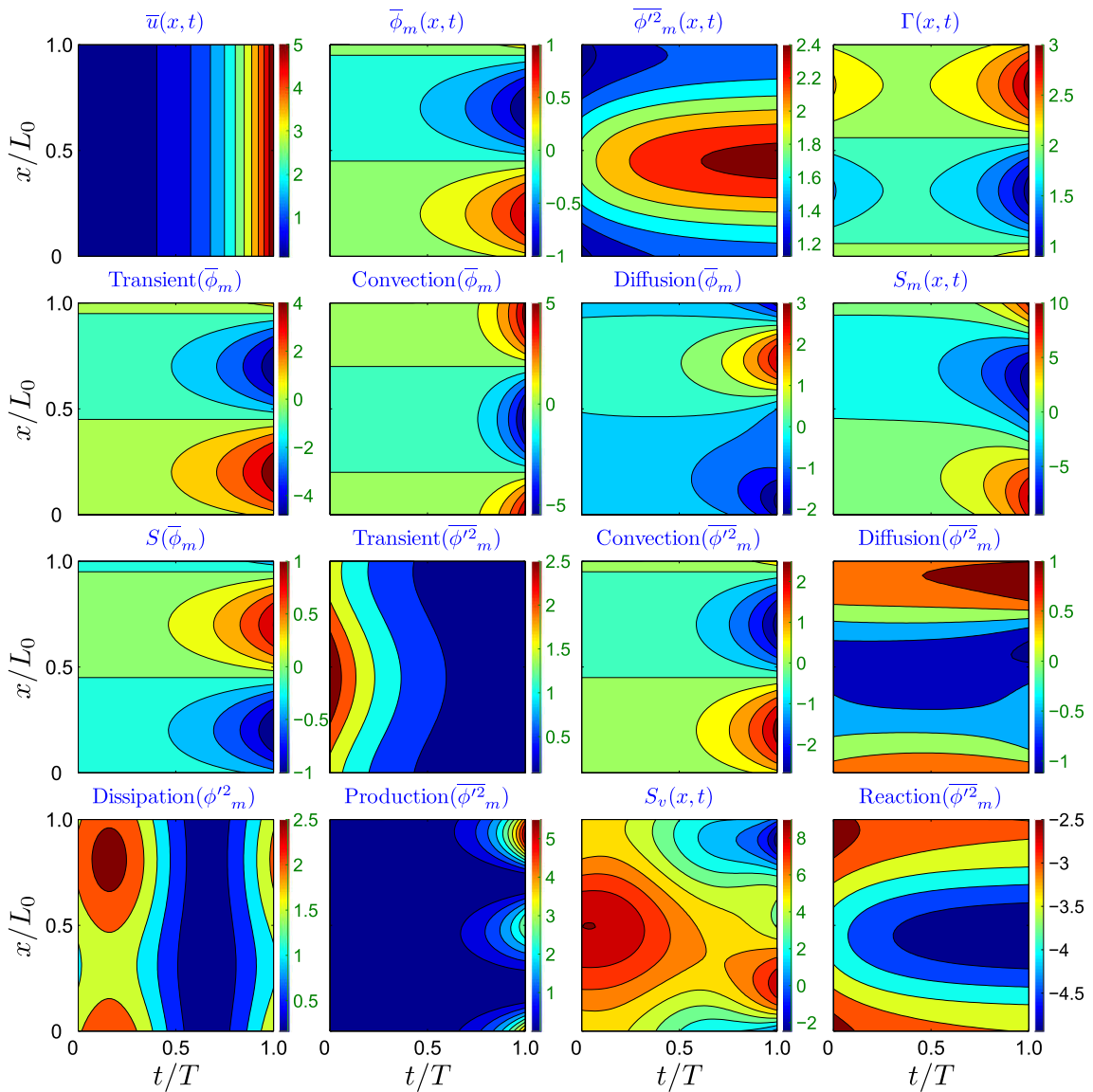The second moment of the scalar $\overline{\phi^2}_m(x,t)$ is then

$$\overline{\phi^2}_m(x,t) = \overline{\phi}_m^2(x,t) + \overline{\phi'^2}_m(x,t). \tag{C.3}$$

The velocity, diffusivity and source terms in (4.2) and (4.3) are specified as follows:

$$\bar{u}(x,t) = \frac{1}{10} u_0 e^{4\varpi t}, \tag{C.4}$$

$$\Gamma(x,t) = \Gamma_0 \left\{ 2 + \frac{2}{5} \left[\sin\left(2\pi\kappa x - \frac{28}{25}\pi \right) \Gamma_x - \Gamma_x + 1 \right] \left(\frac{1}{20} e^{4\varpi t} + e^{-4\varpi t} \right) \right\}, \tag{C.5}$$

$$
\begin{aligned}
S_m(x,t) = {} & \frac{3}{20} \varpi e^{3\varpi t} \cos\left(2\pi\kappa x - \frac{12}{5}\pi \right) + \left[\frac{1}{10} u_0 e^{4\varpi t} - \frac{4}{5}\kappa\pi\Gamma_x\Gamma_0 \cos\left(2\pi\kappa x - \frac{28}{25}\pi \right) \left(\frac{1}{20} e^{4\varpi t} + e^{-4\varpi t} \right) \right] \\
& \times \left[-\frac{1}{10}\kappa\pi e^{3\varpi t} \sin\left(2\pi\kappa x - \frac{12}{5}\pi \right) \right] + e^{3\varpi t} \cos\left(2\pi\kappa x - \frac{12}{5}\pi \right) \\
& \times \left\{ \frac{R_a}{20} + \frac{2}{5}\Gamma_0\kappa^2\pi^2 \left[1 + \frac{1}{5}\left(\sin\left(2\pi\kappa x - \frac{28}{25}\pi \right) \Gamma_x - \Gamma_x + 1 \right) \left(\frac{1}{20} e^{4\varpi t} + e^{-4\varpi t} \right) \right] \right\},
\end{aligned} \tag{C.6}
$$

Fig. C.1. Contour plots of the MMS functions $\bar{u}(x,t)$, $\bar{\phi}_m(x,t)$, $\overline{\phi'^2}_m(x,t)$, $\Gamma(x,t)$ and each term of the augmented transport equations for the scalar mean (4.2) and variance (4.3) with respect to $(x/L_0, t/T)$.

$$
\begin{aligned}
S_v(x,t) =& \frac{3}{8}\varpi e^{-3\varpi t}\left[\sin\left(2\pi\kappa x - \frac{12}{5}\pi\right) + 4\right] \\
&+ \left[\frac{1}{40}u_0\kappa\pi e^{4\varpi t} - \frac{1}{5}\kappa^2\pi^2\Gamma_x\Gamma_0\cos\left(2\pi\kappa x - \frac{28}{25}\pi\right)\left(\frac{1}{20}e^{4\varpi t} + e^{-4\varpi t}\right)\right] \\
&\times (4 - e^{-3\varpi t})\cos\left(2\pi\kappa x - \frac{12}{5}\pi\right) + \Gamma_0\left\{1 + \frac{1}{5}\left[\sin\left(2\pi\kappa x - \frac{28}{25}\pi\right)\Gamma_x - \Gamma_x + 1\right]\left(\frac{1}{20}e^{4\varpi t} + e^{-4\varpi t}\right)\right\} \\
&\times \left\{\kappa^2\pi^2(4 - e^{-3\varpi t})\sin\left(2\pi\kappa x - \frac{12}{5}\pi\right) - \left[-\frac{1}{5}e^{3\varpi t}\sin\left(2\pi\kappa x - \frac{12}{5}\pi\right)\kappa\pi\right]^2\right\} \\
&+ \frac{1}{5}\left[\cos\left(2\pi\varpi t - \frac{1}{5}\pi\varpi\right) + \frac{5}{6}\right]\left[\sin\left(2\pi\kappa x - \frac{28}{25}\pi\right) + \frac{51}{10}\right] \\
&+ \frac{1}{4}R_a(4 - e^{-3\varpi t})\left[\sin\left(2\pi\kappa x - \frac{12}{5}\pi\right) + 4\right],
\end{aligned}
\tag{C.7}
$$

$$
\Omega(x,t) = -\frac{1}{10}\left[\cos\left(2\pi\varpi t - \frac{1}{5}\pi\varpi\right) + \frac{6}{5}\right]\left[\sin\left(2\pi\kappa x - \frac{28}{25}\pi\right) + \frac{51}{10}\right]/\overline{\phi'^2}_m(x,t).
\tag{C.8}
$$

From the above specifications, we obtain the SDE coefficients $D(x,t) = \bar{u}(x,t) + d\Gamma(x,t)/dx$ and $b(x,t) = (2\Gamma(x,t))^{1/2}$. The constants are specified as follows:

$$
\varpi = \frac{5}{\pi}, \quad \kappa = \frac{1}{2\pi}, \quad u_0 = \Gamma_0 = \Gamma_x = 1, \quad R_a = -1, \quad R_b = 0, \quad L_0 = 2\pi, \quad T = \frac{\pi}{5}.
$$

The above functions and constants are specified to minimize the difference of each term of the augmented transport equations for the scalar mean (4.2) and variance (4.3), so that each term has approximately equal contribution to the solutions of the scalar mean and variance. The contour plots of the MMS functions and each term of (4.2) and (4.3) are shown in Fig. C.1.

References

[1] S.B. Pope, PDF methods for turbulent reactive flows, Prog. Energy Combust. Sci. 11 (1985) 119–192.
[2] S.B. Pope, Computations of turbulent combustion: progress and challenges, Proc. Combust. Inst. 23 (1990) 591–612.
[3] S.B. Pope, Turbulent Flows, Cambridge University Press, Cambridge, 2000.
[4] N. Peters, Laminar diffusion flamelet models in non-premixed turbulent combustion, Prog. Energy Combust. Sci. 10 (1984) 319–339.
[5] N. Peters, Turbulent Combustion, Cambridge University Press, Cambridge, 2000.
[6] R.W. Bilger, Conditional moment closure for turbulent reacting flow, Phys. Fluids A 5 (2) (1993) 436–444.
[7] A.Y. Klimenko, R.W. Bilger, Conditional moment closure for turbulent combustion, Prog. Energy Combust. Sci. 25 (1999) 595–687.
[8] J. Xu, S.B. Pope, PDF calculations of turbulent nonpremixed flames with local extinction, Combust. Flame 123 (2000) 281–307.
[9] Q. Tang, J. Xu, S.B. Pope, PDF calculations of local extinction and NO production in piloted-jet turbulent methane/air flames, Proc. Combust. Inst. 28 (2000) 133–139.
[10] R.P. Lindstedt, S.A. Louloudi, E.M. Váos, Joint scalar probability density function modeling of pollutant formation in piloted turbulent jet diffusion flames with comprehensive chemistry, Proc. Combust. Inst. 28 (2000) 149–156.
[11] R.R. Cao, S.B. Pope, A.R. Masri, Turbulent lifted flames in a vitiated coflow investigated using joint PDF calculations, Combust. Flame 142 (2005) 438–453.
[12] R.P. Lindstedt, E.M. Váos, Transported PDF modeling of high-Reynolds-number premixed turbulent flames, Combust. Flame 145 (2006) 495–511.
[13] H. Wang, S.B. Pope, Lagrangian investigation of local extinction, re-ignition and auto-ignition in turbulent flames, Combust. Theory Model. (2008), doi:10.1080/13647830802056137.
[14] F. Gao, E.E. O'Brien, A large-eddy simulation scheme for turbulent reacting flows, Phys. Fluids A 5 (1993) 1282–1284.
[15] P.J. Colucci, F.A. Jaberi, P. Givi, S.B. Pope, Filtered density function for large eddy simulation of turbulent reacting flows, Phys. Fluids 10 (2) (1998) 499–515.
[16] F.A. Jaberi, P.J. Colucci, S. James, P. Givi, S.B. Pope, Filtered mass density function for large-eddy simulation of turbulent reacting flows, J. Fluid Mech. 401 (1999) 85–121.
[17] V. Raman, H. Pitsch, R.O. Fox, Hybrid large-eddy simulation/Lagrangian filtered-density-function approach for simulating turbulent combustion, Combust. Flame 143 (1-2) (2005) 56–78.
[18] M.R.H. Sheikhi, T.G. Drozda, P. Givi, F.A. Jaberi, S.B. Pope, Large eddy simulation of a turbulent nonpremixed piloted methane jet flame (Sandia Flame D), Proc. Combust. Inst. 30 (2005) 549–556.
[19] C. Olbricht, F. Hahn, A. Sadiki, J. Janicka, Analysis of subgrid scale mixing using a hybrid LES-Monte-Carlo PDF method, Int. J. Heat Fluid Flow 28 (6) (2007) 1215–1226.
[20] W.P. Jones, S. Navaffo-Martinez, Large eddy simulation of autoignition with a subgrid probability density function method, Combust. Flame 150 (3) (2007) 170–187.
[21] V. Raman, H. Pitsch, A consistent LES/filtered-density function formulation for the simulation of turbulent flames with detailed chemistry, Proc. Combust. Inst. 31 (2007) 1711–1719.
[22] S. James, J. Zhu, M.S. Anand, Large eddy simulations of turbulent flames using the filtered density function model, Proc. Combust. Inst. 31 (2007) 1737–1745.
[23] S.B. Pope, Particle method for turbulent flows: integration of stochastic model equations, J. Comput. Phys. 117 (1995) 332–349.
[24] P.E. Kloeden, E. Platen, Numerical Solution of Stochastic Differential Equations, Springer-Verlag, Berlin, 1992.
[25] R. Cao, S.B. Pope, Numerical integration of stochastic differential equations: weak second-order mid-point scheme for applications in the composition PDF method, J. Comput. Phys. 185 (2003) 194–212.
[26] E. Platen, On weak implicit and predictor–corrector methods, Math. Comput. Simulat. 38 (1995) 69–76.
[27] K. Burrage, T. Tian, Predictor–corrector methods of Runge–Kutta type for stochastic differential equations, SIAM J. Numer. Anal. 40 (4) (2002) 1516–1537.

[28] J.R. Klauder, W.P. Petersen, Numerical integration of multiplicative-noise stochastic differential equations, SIAM J. Numer. Anal. 22 (6) (1985) 1153–1166.
[29] M.I. Abukhaled, E.J. Allen, A class of second-order Runge–Kutta methods for numerical solution of stochastic differential equations, Stochastic Anal. Appl. 16 (6) (1998) 977–991.
[30] A. Tocino, J. Vigo-Aguiar, weak second order conditions for stochastic Runge–Kutta methods, SIAM J. Sci. Comput. 24 (2) (2002) 507–523.
[31] A. Rößler, Runge–Kutta methods for Itô stochastic differential equations with scalar noise, BIT Numer. Math. 46 (2006) 97–110.
[32] G.N. Milstein, A method of second-order accuracy integration of stochastic differential equations, Theory Prob. Appl. 23 (2) (1978) 396–401.
[33] A. Greiner, W. Strittmatter, J. Honerkamp, Numerical integration of stochastic differential equations, J. Stat. Phys. 51 (1-2) (1988) 95–108.
[34] V. Mackevičius, J. Navikas, Second order weak Runge–Kutta type methods for Itô equations, Math. Comput. Simulat. 57 (1) (2001) 29–34.
[35] A. Rößler, Rooted tree analysis for order conditions of stochastic Runge–Kutta methods for the weak approximation of stochastic differential equations, Stochastic Anal. Appl. 24 (2006) 97–134.
[36] T.H. Tian, K. Burrage, Two-stage stochastic Runge–Kutta methods for stochastic differential equations, BIT 42 (3) (2002) 625–643.
[37] A. Rößler, Second order Runge–Kutta methods for Stratonovich stochastic differential equations, BIT Numer. Math. 47 (2007) 657–680.
[38] C.D. Pierce, P. Moin, Progress-variable approach for large-eddy simulation of turbulent combustion, J. Fluid Mech. 504 (2004) 73–97.
[39] P.J. Roache, Code verification by the method of manufactured solutions, J. Fluids Eng. 124 (1) (2002) 4–10.
[40] C.J. Roy, Review of code and solution verification procedures for computational simulation, J. Comput. Phys. 205 (2005) 131–156.
[41] C.J. Roy, C.C. Nelson, T.M. Smith, C.C. Ober, Verification of Euler/Navier–Stokes codes using the method of manufactured solutions, Int. J. Numer. Method Fluids 44 (2004) 599–620.
[42] L. Eoça, M. Hoekstra, A. Hay, D. Pelletier, On the construction of manufactured solutions for one and two-equation eddy-viscosity models, Int. J. Numer. Method Fluids 54 (2007) 119–154.
[43] L. Eoça, M. Hoekstra, A. Hay, D. Pelletier, Verification of RANS solvers with manufactured solutions, Eng. Comput. 23 (2007) 253–270.
[44] L. Shunn, F. Ham, Method of manufactured solutions applied to variable-density flow solvers, Annual Res. Briefs (2007) 155–168. Center for Turbulence Reseach, Stanford University.
[45] J. Villermaux, J.C. Devillon, Représentation de la coalescence et de la redispersion des domaines de ségrégation dans un fluide par un modèle d'interaction phénoménologique, in: Proceedings of the Second International Symposia on Chemical Reaction, Elsevier, New York, 1972, pp. 1–13.
[46] J. Janicka, W. Kolbe, W. Kollmann, Closure of the transport-equation for the probability density function of turbulent scalar fields, J. Non-Equil. Thermodynam. 4 (1979) 47–66.
[47] S. Subramaniam, S.B. Pope, A mixing model for turbulent reactive flows based on Euclidean minimum spanning trees, Combust. Flame 115 (1998) 487–514.
[48] G. Strang, On the construction and comparison of difference schemes, SIAM J. Numer. Anal. 5 (3) (1968) 506–517.
[49] S.B. Pope, Computationally efficient implementation of combustion chemistry using in situ adaptive tabulation, Combust. Theory Model. 1 (1997) 41–63.
[50] R. McDermott, S.B. Pope, The parabolic edge reconstruction method (PERM) for Lagrangian particle advection, J. Comput. Phys. 227 (2008) 5447–5491.